

Hot-electron transport and ultrafast magnetization dynamics in magnetic multilayers and nanostructures following femtosecond laser pulse excitation

Grégory Malinowski^{1,a}, Nicolas Bergard², Michel Hehn¹, and Stéphane Mangin¹

¹ Institut Jean Lamour, CNRS UMR 7198, Université de Lorraine, 54506 Vandoeuvre-lès-Nancy, France

² Université de Strasbourg, CNRS, Institut de Physique et Chimie des Matériaux de Strasbourg, UMR 7504, 67000 Strasbourg, France

Received 3 October 2017 / Received in final form 22 February 2018

Published online 4 June 2018 – © EDP Sciences, Società Italiana di Fisica, Springer-Verlag 2018

Abstract. Understanding and controlling the magnetization dynamics on the femtosecond timescale is becoming indispensable both at the fundamental level and to develop future technological applications. While direct laser excitation of a ferromagnetic layer was commonly used during the past twenty years, laser induced hot-electrons femtosecond pulses and subsequent transport in magnetic multilayers has attracted a lot of attention. Indeed, replacing photons by hot-electrons offers complementary information to improve our understanding of ultrafast magnetization dynamics and to provide new possibilities for manipulating the magnetization in a thin layer on the femtosecond timescale. In this review, we report on experiments of hot-electrons induced ultrafast magnetic phenomena. We discuss the role of hot-electrons transport in the ultrafast loss of magnetization in magnetic single and multilayers and how it is exploited to trigger magnetization dynamics in magnetic multilayers.

1 Introduction

Manipulating and controlling the magnetic state of a material have been the focus of intensive researches for decades. The desire to understand the physics behind magnetization dynamics was clearly motivated by numerous possible technological applications, such as magnetic hard-disk drives, magnetic memories, and sensors. Within the purpose of ever-increasing the speed and density of data storage and decreasing the energy consumption, different levers were proposed to control the magnetization, for instance magnetic field pulses [1], spin polarized currents [2,3], temperature gradient [4,5], electric fields [6,7], strains [8], and more recently THz excitations [9,10]. Nevertheless, the demonstration of magnetization quenching within less than a picosecond following femtosecond laser pulse excitation [11] together with the possibility of reversing the magnetization using femtosecond polarized laser pulses [12,13], opened up the new field of femtomagnetism. Aside from understanding the microscopic processes involved in laser induced ultrafast magnetization dynamics, the main challenge is to reliably change the magnetic state of a single ferromagnetic structure on the femtosecond timescale.

Concurrently, spintronics revolutionized the field of magnetic memories, magnetic sensors and data storage with the discovery of giant magneto-resistance [14,15] and tunnel magneto-resistance [16]. Following these

breakthroughs, more sophisticated devices such as the spin valve or magnetic tunnel transistors were created [17,18]. These transistors are based on spin-dependent transport of so-called hot-electrons whose energies are well above the Fermi level. As a result, transport properties and relaxation processes of hot-electrons in metals became the subject of intense theoretical and experimental research during the last decades [19,20].

Another way to generate hot-electrons in a metallic material relies on the absorption of a short laser pulse which results in the creation of excited carriers and the formation of electron-hole pairs. Due to the absence of a band-gap in metals, the hot-electrons energy will spread from the Fermi energy up to the excitation energy. The dynamics of photoexcited carriers and their lifetimes was extensively studied by time-resolved two-photon photoemission [21]. In magnetic materials, both the dynamics and life-times of hot-electrons depend on their spin polarization [22–24]. These differences lead to the concept of spin-dependent transport upon laser excitation and thus to the generation of ultrafast spin current pulses. Those femtosecond spin current pulses have attracted a lot of attention since they offer complementary information to improve our understanding of the basic mechanisms responsible for the ultrafast magnetization dynamics. They give as well new possibilities for manipulating a magnetization in a thin layer on the femtosecond timescale.

In the present review, we summarize the recent results regarding ultrafast magnetization dynamics induced by

^a e-mail: gregory.malinowski@univ-lorraine.fr

hot-electron pulses. We first report on the different experimental techniques used to reveal the role of spin-polarized hot-electron transport upon laser excitation and to probe hot-electron induced ultrafast magnetization dynamics. We then briefly describe electronic transport following femtosecond laser pulse excitations, underlining the transition from ballistic to diffusive transport. In the last part, we report experimental results regarding the role of hot-electrons on the ultrafast magnetization dynamics in magnetic single and multilayers. We finally present recent experiments showing how a pulse of spin-polarized hot-electrons can be used to trigger magnetization precession via spin transfer torque effect.

2 Experimental techniques to probe laser and hot-electrons induced ultrafast magnetization dynamics

In this part, we briefly describe some of the experimental time-resolved techniques and set-up that were used to probe laser induced ultrafast demagnetization. We aim at exposing the complementarity of techniques based either on table-top sources or large scale facilities. We will lay emphasis on their ability to disentangle local [25–27] and nonlocal [28,29] contributions to the loss of magnetization. Time-resolved experiments on the femtosecond time scale are usually performed in a pump-probe scheme in which infrared (IR) femtosecond laser pump pulses excite the sample while short probe pulses record the transient magnetic state. The magnetization dynamics is acquired directly in the time domain by varying the delay between the pump and the probe pulses. The femtosecond probe pulses can be generated either by femtosecond pulsed laser [30], at synchrotron [31] or at X-ray free electron laser (XFEL) sources [32]. Usually, stroboscopic acquisition mode is required which limits the investigations to reversible phenomena only. This limitation is overcome either by using the intense photon flux provided by XFEL sources [33] or table-top femtosecond X-ray pulses, which allows single-shot imaging [34].

In the first part of this section, we start describing set-ups based on femtosecond laser sources, referred as table-top experiments. Then, we discuss the time-resolved spectroscopies performed at large scale facilities such as synchrotrons or XFEL sources. In the third part, we present time-resolved imaging techniques, either in the direct or reciprocal space, with lateral spatial resolution.

2.1 Time-resolved experiments on table-top laser sources

The awakening of femtomagnetism arose from the discovery of laser induced sub-picosecond demagnetization in Ni layers by means of time-resolved magneto-optical Kerr effect (TR-MOKE) [11]. In this pioneer experiment, Beaurepaire et al. monitored the intensity of the 60 fs laser pulses reflected by a Ni layer as a function of the delay between the pump and probe pulses. This major breakthrough was followed by an important question: is there a non-magnetic contribution in this kind of TR-MOKE

experiments [35,36]? Koopmans et al. have reported disparate pump induced modification of the Kerr rotation and Kerr ellipticity in the first hundreds of femtoseconds following the laser excitation [35]. They argued that non-magnetic artifacts, such as bleaching effects, dominate the MO responses and casted doubts on genuine spin dynamics on this time scale. Later on, Guidoni et al. derived the transient diagonal and non-diagonal elements of the dielectric tensor in a CoPt₃ film by using pump-probe polarimetry [37]. Their measurements have shown that the transient MOKE signal upon laser excitation is dominated by spin dynamics as long as hot-electrons are thermalized. They have also shown that spin dynamics occurs during the hot-electrons thermalization and that the dynamics can be retrieved in the ultrafast loss of MO contrast. Nowadays, even if the ultrafast spin dynamics is largely admitted, the separation of electron and spin dynamics in the TR-MOKE signal is far from trivial [38,39]. Recently, Razdolski et al. listed the different physical processes that affect the electron distribution in ferromagnetic (FM) layers after laser excitation and proposed a procedure to retrieve the genuine magnetization dynamics from the TR-MOKE signal [40]. Nevertheless, the development of femtomagnetism has strongly benefited from the versatility of TR-MOKE and time-resolved magneto-optical Faraday effect, its transmission counterpart [38,41–47].

The main assets of TR-MOKE reside in the ultrashort pulse duration (≈ 10 fs) and the relative simplicity of the experimental set-up. In its most basic configuration, a beam-splitter separates the laser pulses at the output of a femtosecond laser to generate intense pump pulses and weak probe pulses while a delay line is used in order to control the pump-probe delay. After the reflection on (or transmission through) the magnetic layer, the polarization of the probe pulses is analyzed. Different detection schemes can be used to extract the magnetic signal such as a crossed-polarization, balanced photodiodes, or polarization modulation. A detailed presentation of these different approaches can be found in reference [48]. The laser induced quenching of magnetic order affects both the rotation and ellipticity of the laser polarization and thus the ratio between the s and p part of the reflected (transmitted) probe pulses. The versatility of TR-MOKE makes measurements under ultrahigh vacuum environment, intense magnetic field or/and at low temperatures possible [49–51].

For wavelength centered on the fundamental of routinely used Ti-Sa lasers (800 nm), the magnetic contrast of the MOKE signal is dominated by the 3d spins in transition metals (TM) [52] and 5d spins in rare-earth metals (RE) [53]. The itinerant character of these d electron bands in these metals makes element selectivity very challenging: in TM [54] (RE [55]) based alloys, the ultrafast dynamics of 3d (5d) spins of the different species contribute generally to the TR-MOKE signal. In RE-TM alloys the transient MOKE signal arises mainly from the 3d spin dynamics [56,57]. The probed thickness of the magnetic layer is limited by the light penetration depth, which depends both on the materials and on the wavelength. Typically, for metals at wavelengths in the near-IR and visible part of the spectrum, the latter is in the order

of 10 nm. The wavelength of the probe pulses is tunable by using non-linear crystals such as Beta-Barium-Borate (BBO) or an optical parametric amplifier (OPA) [58]. This allows probing, for instance, particular resonance in oxides [50]. Element selectivity in RE-TM alloys is also achievable in TR-MOKE experiments by tuning the probe wavelength as claimed by Khorsand et al. [59] although it was recently contested by Hassdenteufel et al. [60]. However, a careful analysis of the transient Kerr rotation θ and Kerr ellipticity ϵ gives valuable information: under certain conditions, a separation between different elements contributions [61] and in-depth sensitivity [45,62] can be achieved. In both cases, the experimental methods consist in recording both the transient Kerr rotation θ and Kerr ellipticity ϵ . Schellekens et al. [61] performed TR-MOKE experiments on a Pt(4)/Fe(5)/Ru(1.2)/Ni(5)/Pt(1) magnetic bilayer by varying the axis of a quarter wave plates (QWP) in respect with the photo-elastic modulator (PEM). This procedure allows monitoring the Kerr vector $\Phi = \theta + i\epsilon$ projected on different axis. They found particular positions of the QWP for which the projection axis is orthogonal either to the Ni or Fe Kerr vector removing its contribution from the measured magneto-optical (MO) signal [61]. Such treatment is efficient for chemical selectivity as long as the phase of the Φ vector differs for the different species which is usually the case [63]. Wieczorek et al. have monitored both the transient $\theta(t)$ and $\epsilon(t)$ as a function of the thickness of a Co layer deposited on Cu(001). The different in-depth sensitivity of both θ (near surface) and ϵ (bulk) allows deriving the in-depth magnetization profile [45].

So far, we discussed the contribution of linear MO responses to the signal generated during TR-MOKE measurements. The pioneer experiment performed by Beaurepaire et al. on Ni [11] was shortly followed by a pump-probe experiments in which the second-order MO response of Ni film excited by femtosecond laser pulses was monitored [64]. The non-linear second harmonic generation (SHG) of a specimen is namely the conversion of absorbed photons with a frequency ω into photons with a frequency of 2ω . The yield of the second harmonic generation is governed by the second-order optical susceptibility tensor $\chi(2\omega)$ whose elements vanish in a centrosymmetric medium. However, at surface or interface, the inversion symmetry is broken making SHG a surface or interface sensitive tool. In magnetic medium, $\chi(2\omega)$ depends linearly on magnetization which makes Magnetization-dependent SHG (MSHG) a powerful tool to investigate magnetic properties at the surfaces and buried interfaces [65,66]. Time-resolved MSHG (TR-MSHG) has been widely used to monitor $3d$ spin dynamics in TM [67–71] and $5d$ spin dynamics in rare-earth (RE) [72,73] with surfaces and interfaces sensitivity. Furthermore, the even part of TR-MSHG signal in respect with magnetization reversal is unaffected by magnetization dynamics while the odd part scales linearly with the magnetization [64]. It allows recording simultaneously the transient electronic distribution (even signal) and magnetization dynamics (odd signal) upon laser excitation [64]. Recently, Chen et al. [71] have exploited TR-MSHG to monitor spin accumulation and spin transfer across the Co/Cu interfaces upon laser

excitation providing a direct trial of the superdiffusive spin transport as proposed by Battiato et al. [28,29].

The experimental set-up before the magnetic layer is similar to the TR-MOKE set-up described previously. After the reflection of the probe pulses on the magnetic layer, the SHG yield is separated from the fundamental beam by inserting a dichroic mirror. In this case, the fundamental part of the reflection (at ω) is transmitted while the harmonic (at 2ω) is reflected towards a filter and a grating. The SHG yield is then collected by a photomultiplier and a photon-counter [73].

TR-MOKE and TR-MSHG are versatile tools that have strongly supported the development of femtomagnetism. Parametric amplification allows adjusting the wavelength of the laser pulses on a spectral range varying from the near-IR to visible wavelength. By focusing intense IR femtosecond pulses on a gas cell, it is possible to generate a comb of high harmonic (HHG) with table-top laser sources which allows extending the spectral range to the X-UV [74]. The energy range covers the dipolar transitions from core-level towards conduction band such as the M-edges ($3p \rightarrow 3d$) of transition metals [75] or more recently the N-edges ($4d \rightarrow 4f$) of rare-earth elements [76]. Such sources combine the element selectivity of X-ray based spectroscopies with the sub-100 fs time resolution of laser sources. La-O-Vorakiat et al. have exploited the elements selectivity of these sources to investigate the laser induced dynamics of Ni and Fe $3d$ magnetic moments in permalloy layers [77]. In their experiments, the linearly polarized harmonics were diffracted by a permalloy grating. The harmonic dispersion in energy was recorded as a spatial dispersion on a CCD camera. The magnetic contrast was obtained by comparing the X-ray spectral intensity for two opposite magnetic field directions in a Transverse MOKE configuration. Similar experiments on FeNi alloys were conducted by Matias et al. [78]. In the meanwhile, efficient sources of XUV pulses with elliptical polarization have also been built [79–82]. Willems et al. have performed time resolved Magnetic Circular Dichroism in transmission mode at the Co M and Pt O edges [83]. In their case, the harmonics spectral intensity is also recorded on a CCD camera but the energy dispersion of harmonics is realized through a transmission grating placed behind the probed [Co/Pt] multilayers. Finally, Fan et al. have recorded XMCD spectra at the Gd N_{2,3} and Fe M_{4,5} edges and demonstrated the potential application of their source for time-resolved experiments at RE N-edges [76].

Furthermore, HHG was also used to perform time- and angle-resolved photoelectron spectroscopy [84]. In their experimental set-up, the photon energy was selected by a monochromator design in order to optimize the energy resolution (90 meV) while keeping a decent pulse duration (150 fs) [85]. The photoelectrons were collected in a hemispherical analyzer. Due to the low electron mean free path in metals, these spectroscopies based on photo-electron detection are surface sensitive. In pioneer experiments, Carley et al. used the described set-up to monitor the laser induced modification of epitaxial Gd $5d$ valence band [62]. The authors evidenced different dynamics for minority and majority $5d$ spins. The same group has also explored the laser induced dynamics of $4f$ spins in the

same epitaxial Gd layers by using time-resolved magnetic linear dichroism of Gd $4f$ core levels [86].

2.2 Time-resolved spectroscopy at large scales facilities

The element selectivity and circular polarization make table-top HHG sources valuable tools to deepen the knowledge in femtomagnetism, especially regarding the time resolution and element selectivity. The current developments concerning those source focuses on the covered wavelength range and the prospects tend towards soft X-ray pulses to fill the energy gap with large scale facilities. Such developments are encouraged by the fact that spectroscopic techniques based on X-ray magnetic circular dichroism in the soft X-ray ranges have revolutionized the knowledge on the magnetic properties of thin magnetic layers [87,88]. The L ($2p \rightarrow 3d$) edges of transition metals and the M ($3d \rightarrow 4f$) edges of RE lie in this energy range which allows probing the average $3d$ magnetic moment in transition metals and $4f$ magnetic moments in rare-earth metals. Since XMCD is based on the X-ray Absorption Spectroscopy (XAS), it also provides element selectivity in magnetic alloys [89–91]. Finally, XMCD spectroscopy provides quantitative estimation of the spin and orbital moment thanks to the sum rules analysis [92–95].

The implementation of the femtoslicing operation mode [96] at BESSYII-HZB [97] allowed performing time-resolved XMCD (TR-XMCD) spectroscopy with 100 fs time resolution [98,99]. Since the pioneer experiments on Ni films performed in 2007 by Stamm et al. [100], all the assets of the static XMCD spectroscopy have been transposed in time-resolved version to investigate ultrafast magnetization dynamics. Carva et al. demonstrated the validity of sum rules analysis at the subpicosecond time scale [101]. Subsequently, Boeglin et al. reported laser induced dynamics of the orbital and spin moments in CoPd alloys [102]. Later on, Bergeard et al. extended this study to the L and S dynamics of $4f$ magnetic moments in CoTb and CoGd alloys [103]. Wietstruk et al. evidenced sub-picosecond quenching of $4f$ magnetic order [104] while Radu et al. investigated the laser induced dynamics of Fe $3d$ and Gd $4f$ magnetic moments in amorphous FeCoGd alloys [105]. In these pioneer experiments, the X-ray energy was tuned to core level absorption edges while the transmitted intensity was recorded as a function of the pump-probe delay.

Very recently, Higley et al. published experiments based on TR-XMCD spectroscopy in transmission configuration on GdFeCo alloys performed at the SXR beamline of the linac coherent light source (LCLS) XFEL [106]. The high brilliance of XFEL sources in the soft X-ray energy range allows envisioning time-resolved XMCD experiments on ultrathin magnetic layers or extending the technics to single shot acquisition. Furthermore, the measurement in transmission configuration imposes deposition of magnetic layers on transparent membranes. This limitation is somehow overcome with the advent of time-resolved X-ray resonant magnetic reflectometry (XRMR) [107] at the femtoslicing beamline at BESSYII-HZB. For instance,

Jal et al. used this technique for investigating the magnetization profile upon laser excitation in a polycrystalline Ni layers deposited on a Si substrate [108]. In this experiment, the sample was mounted on a goniometer while the reflected X-ray beam was detected by an avalanche photodiode in a $\theta/2\theta$ configuration. Although the probed thickness of the magnetic layer was given by the X-ray penetration depth, varying the incident angle of the X-ray allowed tuning the ratio between signals coming from the interface and the inner part of the layer. Therefore, this technique offers the possibility to measure the in-depth magnetization profile. As a result, time-resolved XRMR is a valuable tool in order to disentangle the local and non-local mechanisms behind ultrafast demagnetization. Such a technique also enables envisioning investigation of dynamics in magnetic layers displaying more complex magnetic order such as helicoidal magnetic arrangement [109]. Very recently, Rettig et al. have reported time-resolved diffraction experiments performed at the x-ray pump-probe instrument of the LCLS free electron laser by using ultrashort hard X-ray pulses. They have disentangled the laser induced dynamics of $5d$ and $4f$ spins [110].

2.3 Time-resolved imaging at HHG or XFEL sources

In depth profiling by means of TR-MOKE or TR-XRMR allows separating the local and non-local contribution in laser induced ultrafast demagnetization [45,108]. Another more direct way consists in using dichroic diffraction of X-ray short pulses produced at XFEL or HHG sources. Such techniques combine the adequate time and spatial resolutions to investigate the magnetic and chemical properties at the nanometer scale. Among these techniques, time-resolved resonant magnetic small angle X-ray scattering (TR-SAXS) has been widely exploited. In such experiments, a magnetic layer with periodic modulation at the nanometer scale (heterogeneities, magnetic domains) is excited by IR pump pulses while the diffraction patterns of the polarized X-ray probe pulses are recorded on a CCD camera placed behind the sample. In HHG-based pump-probe set-up, the same femtosecond laser is used to generate the XUV probe and the IR pump pulses which makes the experiment almost jitter-free. In that case the time resolution is given by the pulse durations [111]. In FEL based experiments, achieving the ultimate time resolution is much more challenging. The time resolution is deteriorated mainly by the fluctuations of the XUV arrival times intrinsically connected to the emission processes. For instance, in spite of duration below 100 fs for both IR and XUV pulses, Pfau et al. have reported a time resolution of approximately 240 fs at FLASH [112]. Along the past years, several technical solutions were proposed and applied to circumvent this limitation. For instance, these solutions were based on seeding of the electron bunches by XUV pulses [113–115] or on photoionization processes [116,117] in XUV-FEL while optical switching connectors [118] or electronbeam-based alignment [119] were proposed in Hard X-ray FEL. The X-ray photon energy match either the M (FERMI, FLASH,

HHG) or L (LCLS) dichroic absorption edges of transition metals which gives the magnetic contrast and element selectivity. Laser induced modification of the diffraction patterns of labyrinth-like [112,120,121], or stripes magnetic domains [111] as well as chemical heterogeneities at the nanoscale in amorphous alloys [122] have provided valuable information (see Sect. 4.1).

Imaging of the ultrafast dynamics of magnetic domains in direct space with nanoscale resolution is also feasible by means of Fourier Transform Holography [123]. The experimental set-up is based on TR-SAXS taking advantage of the coherence of the X-ray pulses produced in HHG [34,124] or XFEL sources [125,126]. In this case, the transmitted X-ray pulses through the magnetic layer are re-combined with reference X-ray pulses transmitted through a pin-hole. An algorithm is then used in order to retrieve the image from the speckle pattern.

In conclusion, we have briefly presented a non-exhaustive list of experimental set-ups that allow probing the laser induced ultrafast magnetization dynamics. We have limited the discussion on the in-depth resolution and element selectivity of these selected techniques. In Section 4, we will describe how these experimental techniques were operated in order to reveal the contribution of spin-polarized electronic transport during the laser induced ultrafast demagnetization. We would like to mention here the time-resolved two-photon photoemission which has the capabilities to monitor both the photo-excited electronic distribution and the hot-electron lifetime. Although these information are matters of great importance when investigating laser induced spin-polarized hot-electrons transport, we have left this technique aside and we orient the reader towards an exhaustive review on this subject [21].

3 Electronic transport following femtosecond laser pulse excitations

In this section, we shortly describe electronic transport following femtosecond laser pulse excitations, underlining the transition from ballistic to diffusive transport. Then we present the model of superdiffusive transport developed by Battiatio et al. [28,29] to describe ultrafast magnetization dynamics.

3.1 Electronic transport: from ballistic to diffusive

In the early times of ultrafast dynamics triggered by femtosecond laser irradiation, the most common way to describe the space and time evolution of the electron (T_e) and lattice (T_p) temperatures was to use a two temperatures model coupled with heat diffusion,

$$\begin{aligned} C_e[T_e](z, t) \frac{dT_e(z, t)}{dt} &= g_{ep}(T_p(z, t) - T_e(z, t)) \\ &\quad + \nabla_z(\kappa_e \nabla_z T_e(z, t)) + P(z, t), \\ C_p[T_p](z, t) \frac{dT_p(z, t)}{dt} &= g_{ep}(T_e(z, t) - T_p(z, t)) \\ &\quad + \nabla_z(\kappa_p \nabla_z T_p(z, t)). \end{aligned} \quad (1)$$

Equation (1) describes the time dependence of the electron and the lattice temperatures, taking into account the heat diffusion, the coupling to the lattice and the excitation source. C_e and C_p are the electronic and lattice heat capacities, respectively, κ_i represents the thermal conductivity of electrons (e) and phonons (p), g_{ep} is the electron-phonon coupling constant, and $P(z, t)$ is the power density deposited in the sample by the excitation source. While this approach has been heavily used in the past, its main drawback is that it assumes the electronic and lattice systems to be both in thermal equilibrium but having their own temperature. This hypothesis is obviously not correct during the first few hundreds of femtosecond following the laser pulse excitation.

Indeed, the absorption of femtosecond laser pulses triggers the generation of excited carriers formed by electron-hole pairs. Following laser excitations, with typical photon energy of few eV, hot-electrons will move with a speed close to the Fermi velocity which is of the order of 1 nm/fs in metals. In ferromagnetic metals, the transport behavior, such as the inelastic mean free path, lifetime and velocity, strongly depends on the spins [22,24]. As a consequence, hot-electrons with majority spins travel faster and further than hot-electrons with minority spins.

The theory of optically excited hot-electron transport in metals is rather complex due to the effect related to the band structure. Different transport regimes can be characterized by the variance σ^2 of the displacement of a single particle distribution as a function of time which is given by a power law:

$$\sigma^2(t) \sim t^\gamma, \quad (2)$$

where γ is called the anomalous diffusion exponent. Two limits can be distinguished regarding hot-electron transport. On a very short time scale, the transport is ballistic and hot-electrons move in a straight line without experiencing any scattering and so, conserving their angular momentum and energy. It is characterized by $\gamma = 2$. In such a case, hot-electrons move with a constant velocity. In metals, the inelastic lifetime of photo-excited hot-electrons is mainly related to the scattering with unexcited electrons below the Fermi level and is of the orders of few tens of fs. The associated inelastic mean free path can vary from few nm for transition metals due to the presence of the d bands just above the Fermi level to about 100 nm for some noble metals such as Cu, Au and Ag [24].

On a longer timescale, electrons scatter between themselves or with phonon. The movement can be described by a Brownian motion known as standard diffusion and is characterized by an anomalous diffusion exponent $\gamma = 1$. In such a case, unidirectional transport only takes place if a gradient is present which can be thermal, of spin or of charge.

However, both of these limits fail reproducing hot-electron transport and taking into account the intermediate regime becomes a mandatory ingredient. The transient evolution of the anomalous diffusion exponent from 1 to 2 characterizes the superdiffusive regime in which electrons collide a few times before transferring their energy and angular momentum (Fig. 1b). In this situation, not

only the anomalous coefficient is changing but the hot-electrons energy distribution is also evolving. Therefore, the time dependences of both quantities have to be taken into account in order to give an accurate description of hot-electron transport following femtosecond laser pulse excitation.

3.2 Superdiffusive spin transport in metallic heterostructures

In order to understand the role of hot-electron transport on the ultrafast magnetization dynamics, Battiato et al. [28] developed a semiclassical model describing spin-dependent transport in the superdiffusive regime. To do so, they first considered optically excited electrons taking into account the probability distribution of the final energy and the final spin state obtained by *ab initio* calculations and assuming the excitation to be spin-conserving. Since *sp* electrons have a much larger mobility than *d* electrons, the latter are described as quasilocalized and only *sp* electrons are considered to contribute to the transport. Simultaneously to the excitation of hot-electrons, holes are created in the valence band but their mobility being negligible on the relevant timescale, their transport is neglected.

In the calculations, electrons are described as classical particles and start moving ballistically in a random direction after being optically excited. They travel in a straight line until the first scattering event. If they scatter with a phonon or with an impurity, the scattering can be considered as elastic. The electron energy is conserved while its momentum is randomized. Hot-electrons can also scatter with electrons at or below the Fermi energy. In that case, the scattering is inelastic and there is an energy transfer between both electrons depending on the transition probability. After scattering, the electrons keep moving as described previously.

Hot-electrons lifetimes and velocities were taken from *ab initio* calculations [22–24]. Both parameters are materials and energy dependent since they are strongly related to the band structure and their product defines the inelastic mean free path. In a ferromagnetic material, these parameters are spin dependent due to the presence of the exchange splitting. Usually, excited majority carriers possess a longer inelastic mean free path than minority carriers. As a result, they are much more mobile creating a depletion of majority spins at the surface exposed to the laser excitation. When the ferromagnetic layer is in contact with a nonmagnetic metal, excited majority carriers can escape out of a ferromagnetic layer while minority carriers remain trapped as sketched in Figure 1a.

This spin dependent superdiffusive transport induces a modification of the magnetization in the excited area as presented in Figure 1c. Results of the calculation are spread between the two dashed curves due to the dependence of the value on the inelastic mean free path. They correctly reproduce the ultrafast variation of the magnetization measured by time resolved XMCD in a thin Ni film [100]. Therefore, Battiato et al. [28] concluded that superdiffusive transport is a dominant mechanism in the

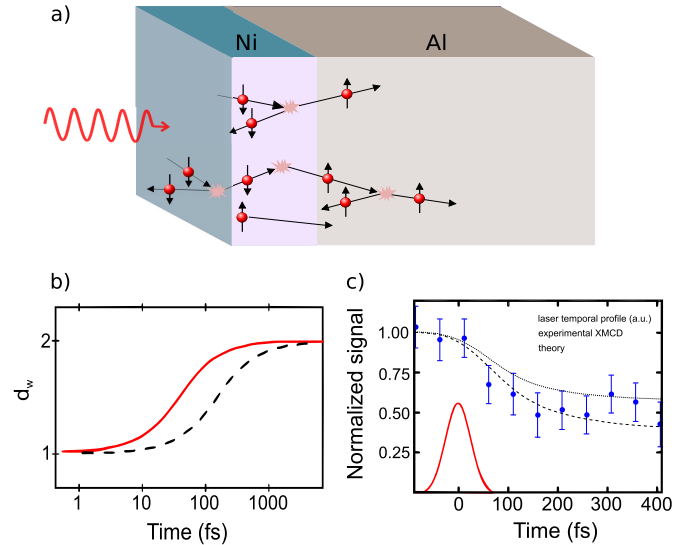


Fig. 1. (a) Schematic representation of spin dependent hot-electron transport in a magnetic heterostructure. The mobile majority carriers move out of the Ni layer leading to a modification of the magnetization. (b) Time dependence of the anomalous diffusion coefficient computed for a particle with constant velocity and an inelastic lifetime of 10 fs (full red curve) or 40 fs (dashed black curve). The anomalous diffusion exponent is given by $\gamma = 2/d_w$ (adapted from [29]). (c) Calculated laser-induced demagnetization in Ni. The results of the calculation vary between both dashed curves depending on the inelastic mean free path. Simulations are compared to experimental results obtained by time resolved XMCD measurements (blue dots) [100] (adapted from Battiato et al. [28,29]). The red solid Gaussian curve represents the temporal structure of the laser pulse used to excite the sample.

process of ultrafast demagnetization during the first few hundred femtoseconds.

As a follow up of this work, they considered typical heterostructures such as presented in Figure 1a but with the idea of comparing a ferromagnetic/nonmagnetic metallic layered junction such as Ni/Al or Fe/Al with a ferromagnetic/nonmagnetic insulator such as Ni/MgO and Fe/MgO [29]. According to their calculations, replacing the metallic layer by an insulating layer constrains the excited carriers within the ferromagnet. Therefore, the average magnetization of the ferromagnet in contact with an insulating layer is conserved. However, the magnetization varies with the depth of the ferromagnet, the region close to the surface excited by the laser being demagnetized due to an accumulation of minority spin carriers while the area close to the insulating layer showing an increased magnetization due to an accumulation of majority spin carriers. Probing these heterostructures using MOKE should lead to a non-zero demagnetization signal in both cases due to the rather fast magneto-optical sensitivity decay with the sample depth. Therefore, a much larger demagnetization should be observed when the ferromagnetic layer is in contact with a metallic layer.

Recently, a microscopic model based on a spin-dependent Boltzmann equation was developed by

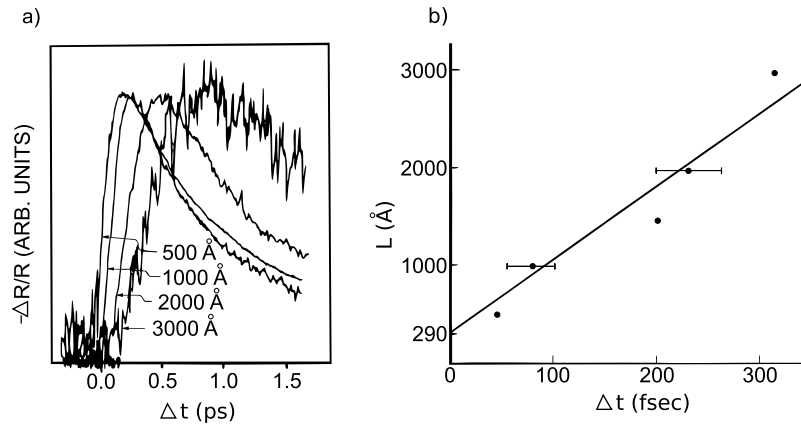


Fig. 2. (a) Variation of the reflectivity at the back side of a Au film of different thicknesses while excited at the front surface. (b) Sample thickness as a function of the time of flight for various Au films of 500, 1000, 15 000, 2000 and 3000 Å thick (adapted from Brorson et al. [137]).

Nenno et al. [127]. In their work, they implemented energy-dependent distributions allowing modeling of the laser excitation while using a parabolic band to describe the dispersion in a nonmagnetic metal. The injection from a ferromagnetic layer into the normal metal (Fig. 3a) was split in two parts, each describing a spin direction. Therefore, only the spin and charge dynamics in a non-magnetic Au layer was modeled. They showed that the injection of holes at the Fe-Au interface could be neglected, leaving only the hot-electrons to enter the Au layer. Furthermore, they showed that in order to understand the spin dynamics, it is mandatory to take into account the energetic distribution of the injected carriers, their velocities as well as the spin dependent scattering. Finally, no modelling of the spin transport in the ferromagnetic layer itself was presented which is of prime importance to correctly calculate the charge and spin dynamics in this system.

In Section 4, we present different experimental studies that tried to quantify the relative contributions of hot-electron transport and local dissipation mechanisms on the ultrafast magnetization dynamics.

4 Hot-electrons induced magnetization dynamics

Since the demonstration by Beaurepaire et al. that a femtosecond laser pulse can quench the magnetization of a 3d metal within less than a picosecond [11], a large amount of researches has been devoted to discover the microscopic processes governing the magnetization dynamics far from equilibrium. For instance, different models have been developed based on a direct coupling between the photon field and the spin bath [44,128], on spin-flip processes induced by electron scattering with particles or quasiparticles [25–27,38,100,129–134], or explaining the loss of magnetization considering thermal mechanisms [135,136]. Transport and relaxation mechanisms of photo-excited carriers in metals have been widely studied for more than 25 years. However, their role on the ultrafast

magnetization dynamics really started to be explored during the last 10 years. In this section, we will first focus on the role played by hot-electron transport in the loss of magnetization within a single ferromagnetic layer and multilayer systems. In a second part, we will review how hot-electron pulses can be used to demagnetize a ferromagnet. Finally, we will look at the case of ultrafast spin transfer torque following hot-electron transport within a magnetic multilayer.

4.1 Ultrafast demagnetization induced by hot-electron transport

The first evidence of ultrafast electronic transport following a laser pulse excitation was observed in a single Au layer by Brorson et al. [137]. The experiment was relatively simple. A Au layer of various thicknesses was deposited on a sapphire substrate. The laser excitation was focused on the front of the sample while probing the change in reflectivity induced at the back by electronic temperature changes. The results are showed in Figure 2a. A clear delay in the onset of the signal was reported when increasing the Au layer thickness (Fig. 2b). However, the delay remained shorter than the electron phonon relaxation time suggesting that the heat transport was carried by electrons that are out of equilibrium. It was lately shown that scattering of the excited electrons depends on the crystal structures of the samples, a larger scattering being observed in polycrystalline samples compared to single-crystals resulting in an average slower effective velocity in the case of thick films [138]. From this moment, it was clear that ballistic and diffusive electronic transports had to be taken into account when dealing with ultrafast laser excitation in metallic systems [139].

In magnetic materials, as presented in Section 3, it was suggested that spin-dependent transport of optically excited hot-electrons could result in a modification of the magnetization due to a redistribution of minority and majority spins within the ferromagnetic layer itself or within an adjacent metallic layer [28]. Following the statement of Battiato et al. that superdiffusive processes play a

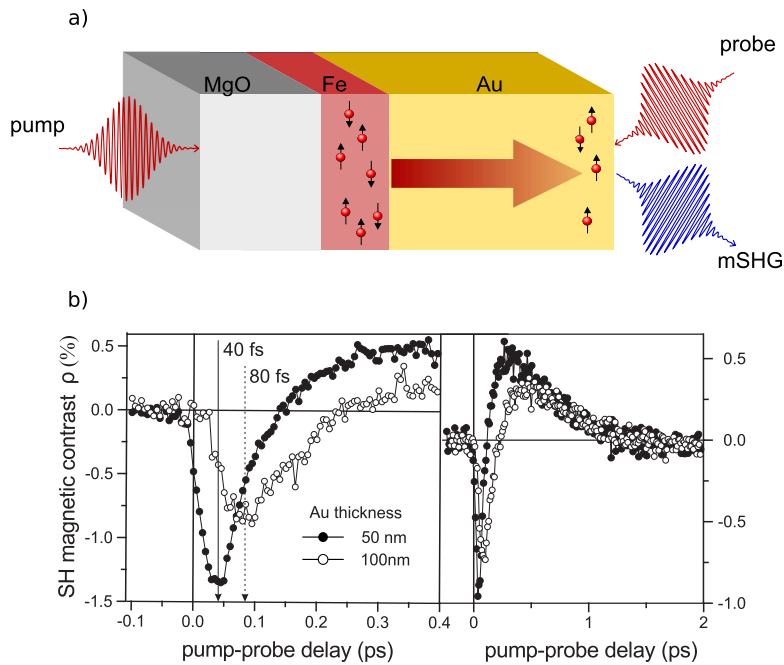


Fig. 3. (a) Schematic representation of the experimental configuration using a back pump excitation and a front probe to measure the magnetic contribution to the second harmonic generation (mSHG) due to hot-electron propagation into a Au layer. (b) Second harmonic magnetic contrast measured at the Au top surface for two different Au thicknesses (adapted from Melnikov et al. [70]).

main role, and can explain wholly the ultrafast demagnetization process during the first few hundred femtoseconds, the quest for experimental demonstration started; even though a clear evidence of the influence of hot-electron transport on the ultrafast magnetization dynamics was already reported by Malinowski et al. [43]. Therefore, researcher tried to quantify the relative contribution of hot-electron transport and local dissipation of angular momentum by spin-flip scattering.

The simplest structure to explore this phenomenon consists of a single ferromagnetic layer. The first attempt to provide an answer to this fundamental question in such a system was undertaken by Melnikov et al. [70]. Using an epitaxial system consisting of Au/Fe/MgO(001), Melnikov and collaborators chose to excite the Fe layer by shining a laser pulse through the MgO substrate. By probing the transient spin polarization at the top Au surface with second harmonic generation, they evidence the existence of a spin-polarized current of hot carriers going from the Fe to the Au layer (Fig. 3). They also showed that the transport was a mixture of ballistic and diffusive propagation due to the energy-dependent hot carriers relaxation times which was found to be about 1 ps.

Later on, a similar approach was undertaken by Schellekens et al. [140]. In order to control the spin transport and verify the prediction of Battiato et al. [29], they grew a Ni thin film on an insulating sapphire substrate and they measured the ultrafast demagnetization by exciting the Ni layer with a laser pulse hitting the front or the back

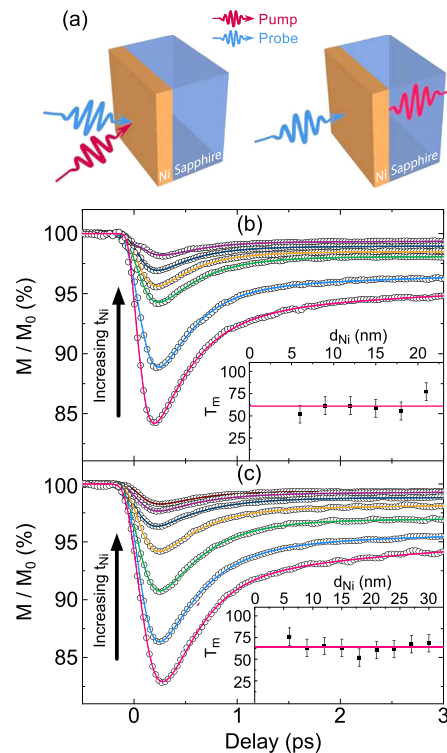


Fig. 4. (a) Schematic representation of the sample excitation and measurement configurations. Magnetization dynamic as a function of the time delay for (b) a front and (c) a back pulsed laser excitation for various thicknesses of a Ni thin film deposited on Sapphire. Insets show the extracted demagnetization times as a function of the Ni thickness (adapted from Schellekens et al. [140]).

of the sample while constantly probing from the front side (Fig. 4a). The idea behind the experiment is the following. In the case of local angular momentum dissipation, both front and back-pump experiments should result in a similar demagnetization. In the case of ultrafast demagnetization induced solely by transport of excited carriers, a front-pump configuration should lead to a decrease of the magnetization due to a flow of majority electrons toward the substrate. When pumped from the samples back side, an increase of the magnetization is expected due to a flow of majority electrons towards the probe spot.

First of all, they showed that both front and back-pump excitations lead to a demagnetization of the Ni layer (Figs. 4b and 4c). By analyzing the demagnetization curves in more details, they extracted the timescale for demagnetization and they found out that there is no difference between the two scenarios. Moreover, they clearly showed that the reduction of the magneto-optical quenching as a function of the Ni thickness can be attributed to a decrease in the absorption when the Ni thickness is increased for both configurations. Therefore, all these results demonstrate that transport plays no significant role in the demagnetization of ferromagnetic Ni thin films on insulating substrates. By combining pump-probe TR-MOKE experiments with time-resolved density functional theory calculations, Shokeen et al. confirmed that

in Ni, spin flips are the main mechanism leading to global demagnetization [141].

In order to confirm those results, they finally grew a thin film of Ni on top of a wedge of Al. In the case of ultrafast demagnetization governed by hot-electron transport, the presence of such a metallic layer should lead to an enhancement of the quenching due to transport of spins outside of the ferromagnet. Results of the measurements showed that the characteristic demagnetization time is not influenced by the presence of the metallic layer. Moreover, increasing the Al thickness results in a decrease of the maximum quenching which does not support a significant role of transport in the demagnetization process of ferromagnetic thin films. More recently, Wieczorek et al. investigated the relative contribution of transport and local angular momentum dissipation in another system, namely Co/Cu(100), using the complex magneto-optical Kerr effect as described in Section 2.1 [45]. By comparing their measurements to calculations based on the microscopic three-temperature model (M3TM) and on spin diffusion equation, they revealed that spin-flip plays a major role in the near-surface region at delays just above 200 fs while spin transport processes are located near the bottom Co-Cu interface and took place on a shorter timescale, earlier than 100 fs at which the hot-electrons are not thermalized yet. Unlike the previous reports in the case of Ni films by Schellekens et al. [102], spin transport processes play a significant role in Co films. Such disparate behavior has been recently confirmed by Shokeen et al. [141].

Surprisingly, the study of Hofherr et al. provides clear evidences of femtosecond injection of spin current from a Ni layer into a metallic Au substrate [142]. They concluded that the demagnetization dynamics in this system is mainly caused by hot-electrons transport. These results are in clear contradiction with previous works presented above. Therefore, it seems essential to start focusing on the role played by the interface in the ability to inject spin-polarized hot-electrons from a ferromagnetic layer into an adjacent nonmagnetic metal.

While the precedent paragraphs were focused on heterostructures containing a single ferromagnetic layer, evidence of hot-electron transport and its influence on the ultrafast demagnetization was mostly studied in magnetic multilayers. In 2008, a pioneering experiment was reported by Malinowski et al. [43]. A schematic description of the experiment and the principal results are reported in Figure 5a. The original idea was to use a multilayer made of two ferromagnetic layers separated by either a metallic layer (Ru) or an insulating layer (NiO) in order to control the hot-electrons flow between them. Laser excited spin-polarized hot-electrons are created in both magnetic layers and travel ballistically from one to the other, transferring angular momentum. In the case of an insulating spacer, no difference in the ultrafast magnetization dynamics was observed between a parallel or antiparallel alignment of the magnetizations. In the case of a metallic spacer, the initial demagnetization is larger and faster in the case of an anti-parallel alignment compared to a parallel alignment. The authors explained this difference by spin-polarized hot-electron flow, allowing for

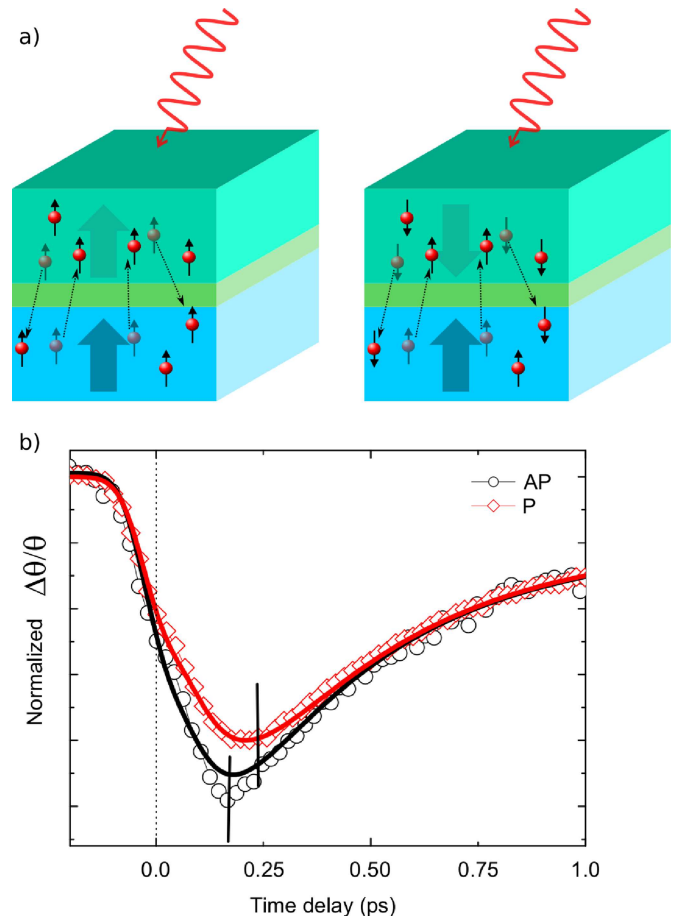


Fig. 5. (a) Schematic representation of laser excited electrons transport in magnetic heterostructures. (b) Normalized Kerr signal measured for parallel (P – diamonds) or antiparallel (AP – circles) alignment of the magnetizations (adapted from Malinowski et al. [43]).

interlayer transfer of spin angular momentum between the ferromagnetic layers (Fig. 5).

Later on, similar results were reported by Wei et al. who studied the ultrafast demagnetization in CoFeB/MgO/CoFeB magnetic tunnel junctions [143]. Beside a more efficient ultrafast demagnetization observed for an antiparallel alignment of both CoFeB magnetizations, they showed that the enhancement due to superdiffusive spin transport increased with increasing the laser fluence before saturating to a maximum value. These results seem contradictory with the results of Malinowski et al. in which no transport of excited electrons was evidenced in the case of a NiO spacer [43]. This could be explained by the different tunneling barriers obtained with MgO and NiO but also by the antiferromagnetic order in the NiO thin layer which might increase the spin scattering.

The advent of ultrafast X-ray and extreme-ultraviolet sources allowed for probing spin dynamics in different magnetic layers within the same heterostructure due to the chemical selectivity (cf Sect. 2.1). Using table-top laser-based high-harmonic generation sources, Rudolph

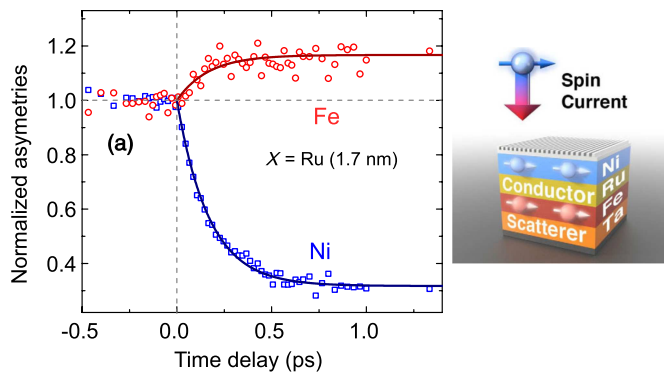


Fig. 6. Layer-selective magnetization dynamics measured by T-MOKE using high-harmonics in substrate / Ta(3nm) / Fe(4 nm) / Ru(1.7 nm) / Ni(5 nm) / Si₃N₄(6 nm) showing a clear enhancement of the Fe magnetization (adapted from Turgut et al. [144]).

et al. simultaneously measured the spin dynamic of Fe and Ni in a Ni/Ru/Fe trilayer [144,145]. One of the most exciting result is reported in Figure 6. As surprising as it might be, femtosecond laser excitation of this system resulted in an increase of the magnetization in the Fe film. This counterintuitive result was attributed to the large superdiffusive majority spin currents flowing from the top Ni layer into the Fe layer while minority spins were mainly trapped in the Ni layer due to their much shorter lifetimes. A detailed interpretation of these results indicates that heating, and therefore spin-flip processes, play a minor role in ultrafast demagnetization dynamics.

The same group performed complementary experiments to disentangle the contributions of spin-flip scattering and spin-transport processes in similar multilayers. In order to modify the ratio between both processes, they used different spacer layers with different spin lifetime or even an insulating Si₃N₄ to fully suppress spin currents [144]. Their results could only be explained by the simultaneous presence of both interlayer spin-current flow and spin-flip processes. By inverting the Ni and Fe layer in the structure, they have also noticed that the spin current is directional. Indeed, it preferentially flows towards the bottom of the sample. A plausible explanation would rely on the fact that the top interface would reflect the spins while the Ta seed layer would act as a strong spin scatterer, therefore reducing the majority spins flowing from the buried ferromagnetic layer. Another explanation might be related to the occurrence of time dependent thermal gradient due to the absorption profile of the laser pulse within the multilayer.

Schellekens et al. investigated the same structure by TR-MOKE using a material- and/or depth-resolved technique (cf Sect. 2.1) [61]. They could access to both layers magneto-optical signal independently (Fig. 7a) and measured the ultrafast magnetization of both Ni and Fe layers (Figs. 7b and 7c). Their results unambiguously showed a more effective and faster demagnetization when both layers magnetizations are antiparallel. They estimated that roughly 30% of the Ni demagnetization was due to superdiffusive spin currents coming from the Fe layer.

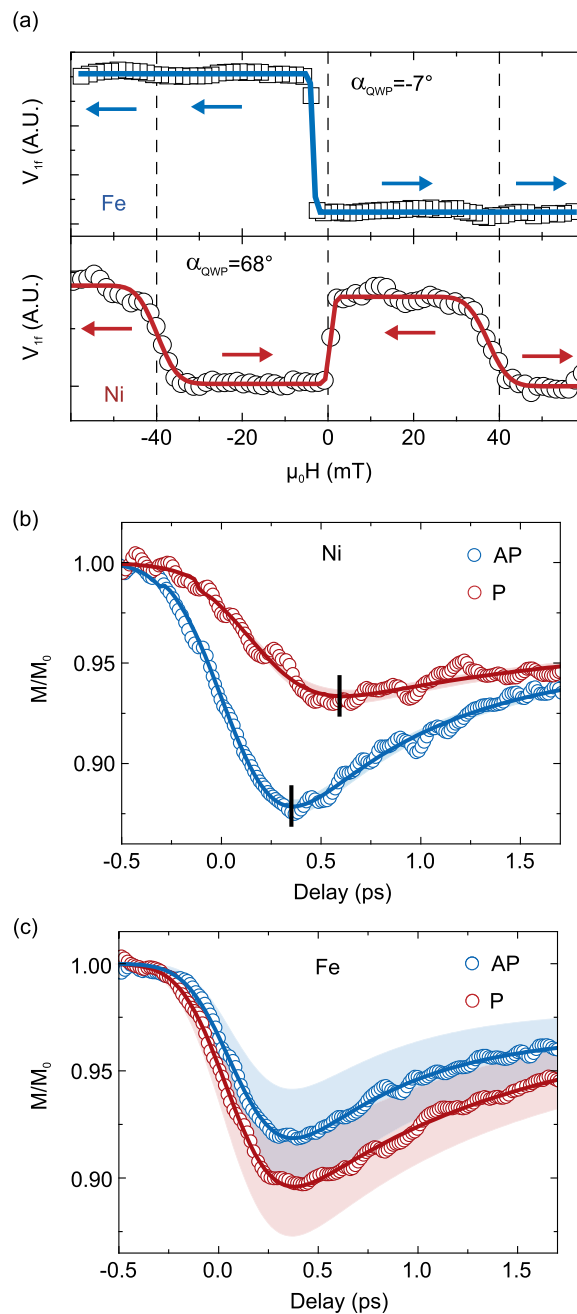


Fig. 7. (a) One branch of the hysteresis loop is shown for an angle of the quarter wave plate (QWP) $\alpha = -7^\circ$, showing only the contribution to the MO contrast from Fe and the same is shown in the case of $\alpha = -68^\circ$, showing only the contribution to the MO contrast from Ni. Demagnetization traces of Ni (b) and Fe (c). The lines are fit to the data and the shaded areas represent the errors due to the mixing of the Ni and Fe MO signals (adapted from Schellekens et al. [61]).

However, a major difference with the results reported by Rudolph et al. was pointed out. They did not observe an ultrafast increase of the Fe magnetization. Moreover, they found that the Fe transient demagnetization was similar for both parallel and antiparallel alignments, casting doubt on the superdiffusive spin transport contribution.

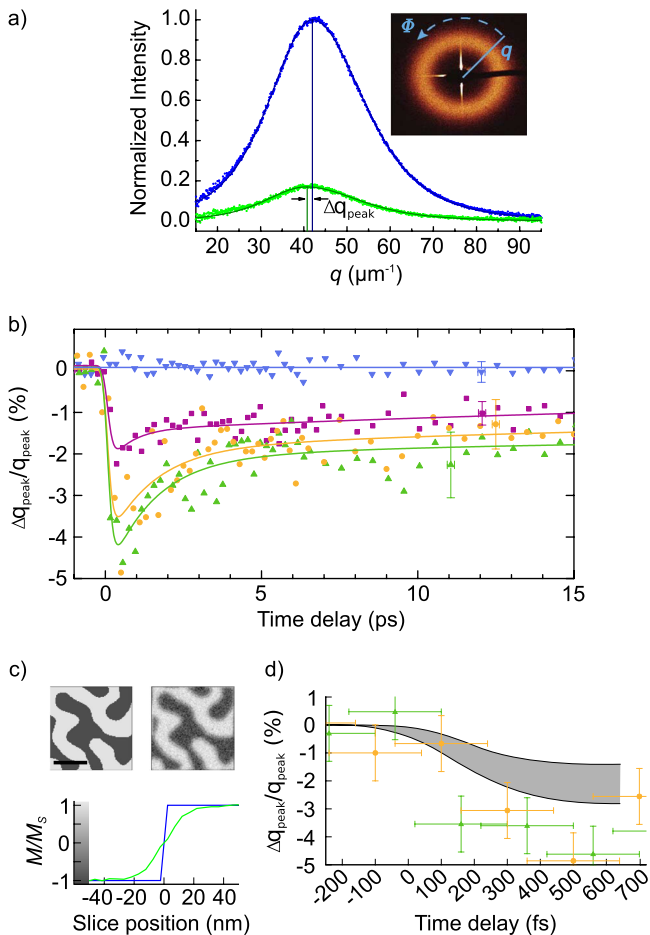


Fig. 8. (a) Azimuthally integrated SAXS intensity (see inset) probed by a delayed X-ray pulse produced by the FEL. (b) Time evolution of the shift of the integrated SAXS maximum intensity. (c) Temporal evolution of the magnetization in a selected area at the start (top left) and after 300 fs (top right) calculated by Monte-Carlo simulation of the superdiffusive spin-transport (scale bar, 200 nm) and resulting domain-wall profile (bottom). The blue line corresponds to the initial profile while the green one is obtained after 300 fs. (d) Temporal evolution of the shift of the SAXS maximum intensity obtained by simulation (line) and from the experiment (points and error bars). The grey area reflects the uncertainties of the simulations (adapted from Pfau et al. [112]).

Even though the magnetic multilayers were similar, both studies were performed for different laser fluences. Indeed, a much stronger excitation was used in the work of Rudolf et al. [145]. This might result in a higher spin transport contribution for larger laser fluences [143].

The role of superdiffusive transport was also investigated in single ferromagnetic layers showing a magnetic domain structure. In such a system, magnetic domain walls separate domains with opposite magnetization. Hence, they play a similar role as the spacer that is used in a multilayer structure. However, two principal differences can be pointed out when comparing this with a multilayer approach. First, the sample is chemically homogeneous avoiding therefore any disruption in the band

structure. Second, in this configuration, any effect of ultrafast electronic transport mainly comes from lateral electronic motion.

Pfau et al. used time resolved magnetic small-angle X-ray scattering (SAXS) to study the magnetic response to ultrafast laser excitation of a lateral maze domain pattern [112]. They showed that the SAXS intensity decreases after exposure to laser excitation which reflects the decrease of the average domain magnetization. What is more remarkable is the presence of a shift in the momentum transfer showing similar dynamics to the loss of magnetization on the femtosecond timescale (Fig. 8). In order to explain the spatial modification of the maze structure following laser excitation, they proposed that spin-dependent transport of optically excited hot-electrons across the domain walls strongly modifies its magnetization profile, therefore changing the domains scattering form factor.

Using a similar system presenting a nanoscale magnetic domain network, Vodungbo et al. did not observe any modification of the magnetic structure [111]. However, they showed that the demagnetization is significantly faster compared to a uniformly magnetized system of similar composition. Moreover, the characteristic demagnetization time has been shown to be independent of the amplitude of magnetization quenching in contradiction with experimental reports on similar systems uniformly magnetized [146]. To explain these results, they also came to the conclusion that there is a direct spin angular momentum transfer between neighboring domains.

In order to verify this explanation, Moisan et al. investigated the dynamics of similar samples for different magnetic configurations. By changing the applied magnetic field during the experiment, they modified the magnetic domain structure going from a periodic system in the absence of magnetic field to a fully saturated system at high magnetic field. In the case of an intermediate magnetic field, one kind of domain was favored and these domains expanded at the expense of the other. The presence of hot-electron spin transport between neighboring domains should result in the alteration of the demagnetization dynamics and in a larger demagnetization amplitude. However, no contribution either to the characteristic demagnetization time or to the demagnetization amplitude was observed. Therefore they concluded that the demagnetization was mainly due to spin flip processes.

Although the spin-polarized transport of hot-electrons plays a significant role on the time scale required for hot-electrons thermalization, the huge experimental efforts provided so far have shown that such mechanism alone cannot explain the whole complexity of laser induced demagnetization.

4.2 Ultrafast magnetization dynamics induced by unpolarized hot-electrons

New interest in the role of hot-electrons transport has emerged since Eschenlohr et al. reported sub-picosecond magnetization dynamics induced by optically generated hot-electrons [147]. The authors used IR laser pulses to

excite an out of equilibrium distribution of hot-electrons in a Au(30 nm) layer deposited on top of a Ni(15 nm) layer. The Au capping layer was supposed to absorb more than 90% of incident IR laser pulses and thus to avoid direct laser excitation in the buried Ni layer. The subsequent magnetization dynamics of the Ni layer, as well as the direct laser induced dynamics in an uncapped Ni thin film used as reference, were monitored by time-resolved XMCD at the femtoslicing beamline at BESSYII (Fig. 9). The laser fluences for the capped and uncapped samples were tuned in order to ensure equivalent absorbed energy. The authors reported ultrafast quenching of the $3d$ magnetic order in the Ni layer for both the direct and indirect IR laser excitation, with similar demagnetization amplitudes and characteristic times. In the case of indirect excitation, they have attributed the demagnetization to the excited hot-electrons transport from the Au layer towards the Ni layer. The slight delay revealed by the comparison of the direct and indirect excitations was attributed to the time required for the hot-electrons to cross the Au layer before interacting with the Ni magnetization. Their scenario was corroborated by numerical calculation based on the superdiffusive spin transport theory of hot-electrons [28,148]. The authors concluded that the direct interaction of IR photons with the electronic bath of the excited magnetic material is not the only source of ultrafast dynamics and those hot-electrons are as efficient as direct IR laser excitation to induce demagnetization. However, the interpretations extracted from these exciting pioneer results were contested due to the under estimation of transmitted light through the Au capping layer.

Later on, Eschenlohr's conclusions were strengthened by Vodungbo et al. who performed time-resolved resonant magnetic small-angle X-ray scattering, at the SXR instruments (LCLS-Stanford), on two ferromagnetic (Co0.4 nm/Pd0.2 nm) \times 30 multilayers (ML) capped either with Al(3 nm) or with Al(40 nm) [121]. The former is referred as the uncapped ML while the latter is referred as the capped ML. The authors made sure that the IR intensity transmitted through the Al(40 nm) capping layer was negligible. The uncapped Co/Pd ML presented a conventional demagnetization upon direct laser excitation, similar to what was previously measured in such samples [102,111]. On the contrary, the capped Co/Pd ML showed a delayed onset, a lower demagnetization amplitude, and a slower demagnetization rate (Fig. 10). Following Eschenlohr's claim [147], they attributed these features to the hot-electrons induced demagnetization in the capped ML. The discrepancies between both studies [147], such as the slower demagnetization rate and the longer delay for the demagnetization onset, were attributed to both the broadening of the electron distribution and the thicker capping layer. Although in qualitative agreements in respect with the overall scenario, Vodungbo et al. remained cautious regarding the mechanisms by which the hot-electrons triggered the demagnetization in the buried Co/Pd ML. They also pointed out that the shorter hot-electron life time in Al compared to Au could be responsible for the pulse stretching. This work has definitely settled the controversy raised by Khorsand et al. [149] concerning the hot-electrons induced demagnetization but it has called

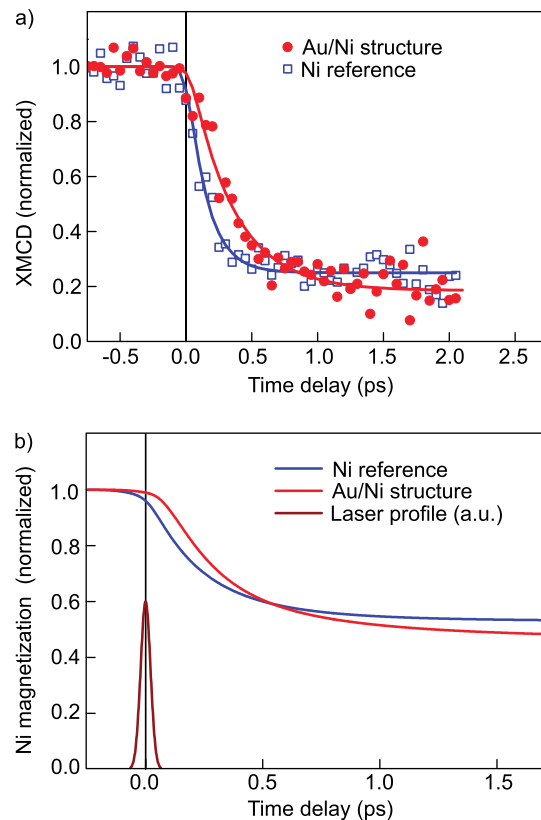


Fig. 9. (a) Time evolution of the magnetization of Ni reference sample (open symbols) and Au/Ni sample (filled symbols) after excitation with a femtosecond laser pulse. (b) Calculated time evolution of the average magnetization of the Ni film, in the Ni reference layer and Au/Ni sample (adapted from Eschenlohr et al. [147]).

for further investigations to reveal the transport regime of hot-electrons and the microscopic mechanisms that allow transferring angular momentum on the femtosecond time-scale.

Bergeard et al. [46] and Salvatella et al. [47] published almost simultaneously investigations of hot-electrons induced demagnetization performed by tuning the thickness of the non-magnetic capping layers. In both reports, the data acquisition was based on table-top time-resolved magneto-optical Kerr effect (TR-MOKE) which is well suited for such systematic investigations. In the former publication, the authors have investigated Pt(3 nm)/Cu(d nm)/[Co/Pt](4 nm) multilayers (Fig. 11a) while in the latter, the authors have investigated Al(d nm)/Ni(10 nm) bi-layers. Both studies revealed a thickness of the capping layer ($d_{Cu} = 60$ nm and $d_{Al} = 30$ nm) at which the direct laser excitation of the magnetic layer is ruled out and above which hot-electrons induced demagnetization became predominant. On one hand, Bergeard et al. have reported a linear dependence of the onset of demagnetization with the Cu thickness over the investigated range (Fig. 11b). This was attributed to ballistic transport of hot-electrons [137,138]. The characteristic features of the demagnetization were successfully simulated by using the microscopic 3 temperatures model [26] in which a source

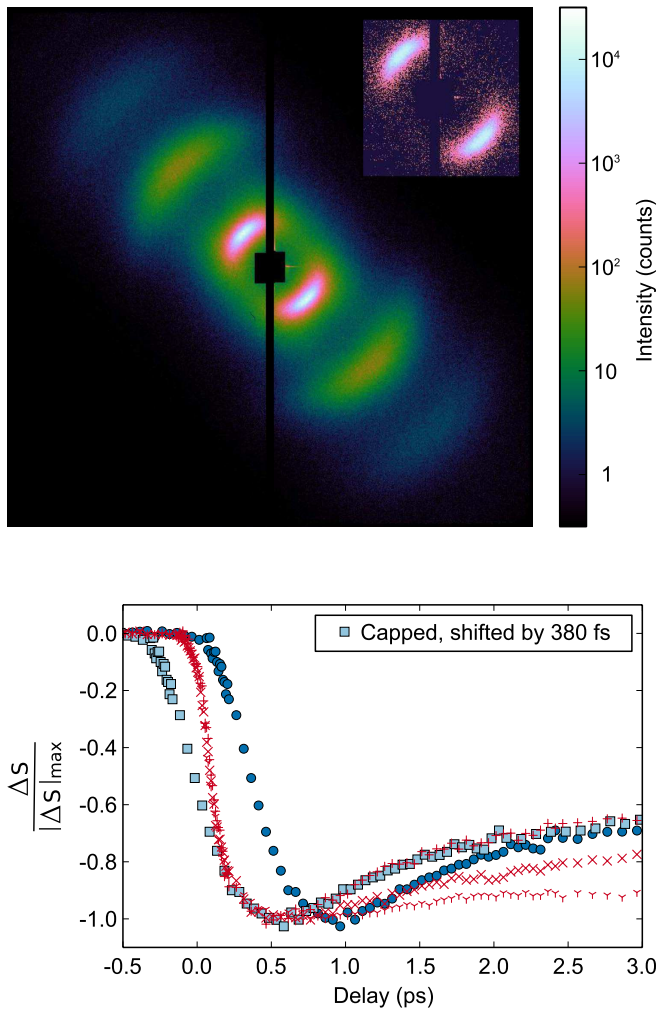


Fig. 10. (a) Resonant magnetic scattering pattern recorded at the Co L3 edge. The pattern in inset was obtained with a single X-ray pulse. Averaging over about thousands shots reveals scattering up to the fifth order (even orders are suppressed). (b) Normalized magnetic scattering intensity as a function of the delay for capped (blue symbols) and uncapped (red symbols) samples (adapted from [111]).

term was implemented taking into account a ballistic hot-electrons pulse [46]. On the other hand, Salvatella et al. reported a slope break in the thickness dependence of the characteristic demagnetization times at $d = 30$ nm [47]. This behavior was attributed to diffusive heat transport by hot-electrons. Their interpretation was supported by solving the diffusion equation.

Few experimental investigations of hot-electrons induced demagnetization have been carried out up to now, but they have nonetheless revealed that the direct laser excitation is not a prerequisite to achieve ultrafast demagnetization and that hot-electron induced demagnetization is as efficient as laser induced demagnetization. These studies have also pointed out that the materials used to transport the excited electrons determine their transport regime, diffusive for Al [47,121] or ballistic for Cu [46]. Nevertheless, the discussion concerning the

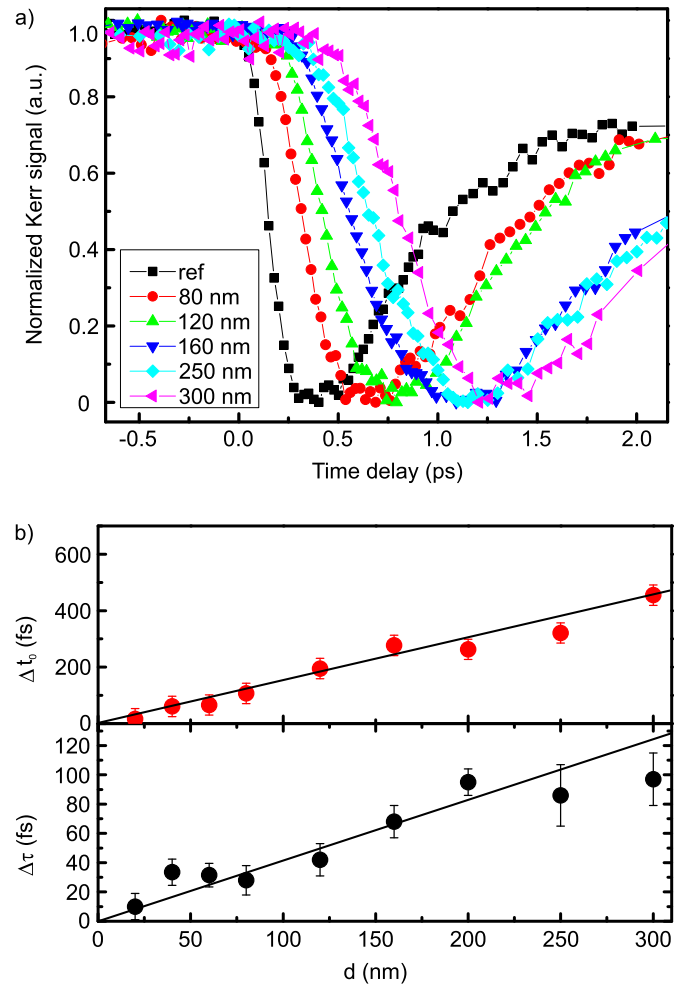


Fig. 11. (a) Time evolution of the normalized Kerr signal for different Cu thickness. (b) Cu thickness dependence of the induced delay in the onset of demagnetization (top) and of the characteristic demagnetization time (bottom) (adapted from Bergerard et al. [46]).

microscopic mechanisms that allows transferring angular momentum on the sub-picosecond time scale is far from being solved since both the non-local superdiffusive spin transport [28,147,148] and the local microscopic 3 temperatures models [26,46] were invoked.

4.3 Manipulation of spin with hot-electrons: towards femtosecond spintronics

This growing field of hot-electron induced demagnetization opens the route towards femtosecond spintronics using the spin transfer torque effect [150,151]. In the following, we report recent studies that took advantage of hot-electron transport to not only demagnetize a magnetic film but to manipulate its magnetization. It has been shown almost simultaneously that both ballistic [46] and diffusive [47,121] transport of hot-electrons lead to ultrafast demagnetization. Similarly, manipulation of magnetization by ultrafast spin-transfer torque either by

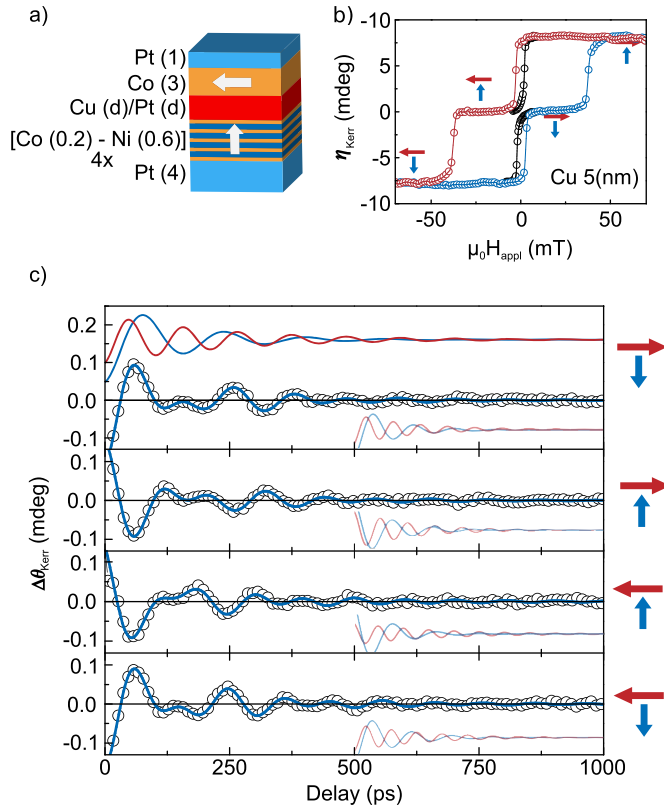


Fig. 12. (a) Structure used to investigate ultrafast STT. (b) Longitudinal MOKE measurements for a 5 nm Cu spacing layer. The field is applied at 30 degrees angle from the film plane. (c) Time-resolved measurements of the out-of-plane component of the magnetization for different magnetic configuration as depicted by the arrows on the right hand-side. Adapted from [154].

ballistic or diffusive hot-electrons were reported by different groups [152–154]. In these articles, femtosecond IR laser pulses were used in order to generate spin-polarized hot-electron pulses that propagate towards a ferromagnetic layer whose magnetization dynamics was recorded by means of TR-MOKE. The authors used spin valves structures in which the first ferromagnetic layer is used as a spin-polarizer while the second magnetic layer is used as a detector (Fig. 12a). Since both experiments aimed at revealing the spin-torque exerted by the spin-polarized hot-electrons on the magnetization of the detector layer, the two ferromagnetic layers possessed crossed magnetic anisotropies, one pointing in the sample plane while the second one being out-of-plane. This crossed configuration enhanced the torque and avoided any threshold, inherent to parallel anisotropies configuration [2].

In the experiment proposed by Schellekens et al. [154], the whole sample was fully excited by the laser pulse, just as in previous experiments [43]. They reported two oscillation regimes that are superimposed with the conventional laser induced demagnetization (Fig. 12c). They presented a detailed investigation by varying the non-magnetic inter-layer and their thicknesses, the amplitude of the magnetic field as well as the magnetic configurations

of both magnetic layers. Finally, they concluded that the precessional phase of the in-plane magnetized layer was determined by the orientation of the out-of-plane magnetized layer, which is fully consistent with an ultrafast laser-induced spin transfer torque. The second contribution was assigned to a precession in the out-of-plane magnetized layer due to a laser induced modification of the local anisotropy. Furthermore, they extracted the amount of angular momentum transferred from the out-of-plane to the in-plane magnetized layer. A maximum of only 2% of the spin participating in the demagnetization of the top out-of-plane layer are absorbed in the bottom layer for a Cu spacing layer of 2 nm. This amount decreases exponentially when the thickness increases due to the enhancement of spin flip scattering with a spin transfer length of about 13 nm for Cu. This length is strongly reduced to 3 nm in the case of Pt.

In the results reported by Choi et al., the fs laser pulses are fully absorbed in the top Pt(30 nm) capping layer resulting in an ultrafast rise of electronic temperature [152,155]. The thermal transport from the excited Pt top layer towards the buried layers trig the demagnetization of the adjacent ferromagnetic [Co/Pt] multilayer as described in the previous section [47,121]. The demagnetization is followed by the emission of spin currents that are used to excite a second CoFeB magnetic layer. Moreover, they showed that spin-dependent Seebeck effect has a significant contribution on the thermal STT because its duration of about 100 ps is far longer than the generation of spin current induced by the magnetization loss (~ 3 ps) as they pointed out in another publication [153]. Finally, they demonstrated that an energy fluence of $\sim 4 \text{ J m}^{-2}$ induces a tilting of the precessing layer of $\sim 1\%$ only. They propose that this efficiency can be increased by controlling the band structure using half-metallic materials for instance.

Razdolski et al. used a similar structure composed of two Fe layers separated by a thick Au layer [156]. A sub-picosecond spin current pulse is generated by exciting the top Fe layer. The magnetization of both Fe layers were orthogonal in order to optimize the torque exerted by the hot-electrons entering the bottom Fe layer. This results in the excitation of spin dynamics in the bottom Fe layer. Due to the very short penetration depth of spin-polarized hot-electrons into the Fe layer, confined high frequency perpendicular spin-waves with non-zero k vectors are excited. From their measurements (Fig. 13), excitations up to the mode $n = 4$ were observed with a frequency as large as 0.56 THz. Therefore, hot-electron induced spin transfer torque is one of the most efficient mechanism for exciting spin-waves with high k vectors. The same group demonstrated that the generation of ultrashort spin current pulses in this sample was related to the existence of a nonthermal spin-dependent Seebeck effect [157]. They give clear evidence of ballistic transport of spin-polarized electrons in the Au layer. Using a sample structure similar to the one presented in Figure 12a, and varying the number of repetitions of the [Co/Ni] multilayer, Laliou et al. showed that the efficiency of STT does not depends on the number of repetition of [Co/Ni] bilayers [158]. In other words, the amount of angular momentum absorbed

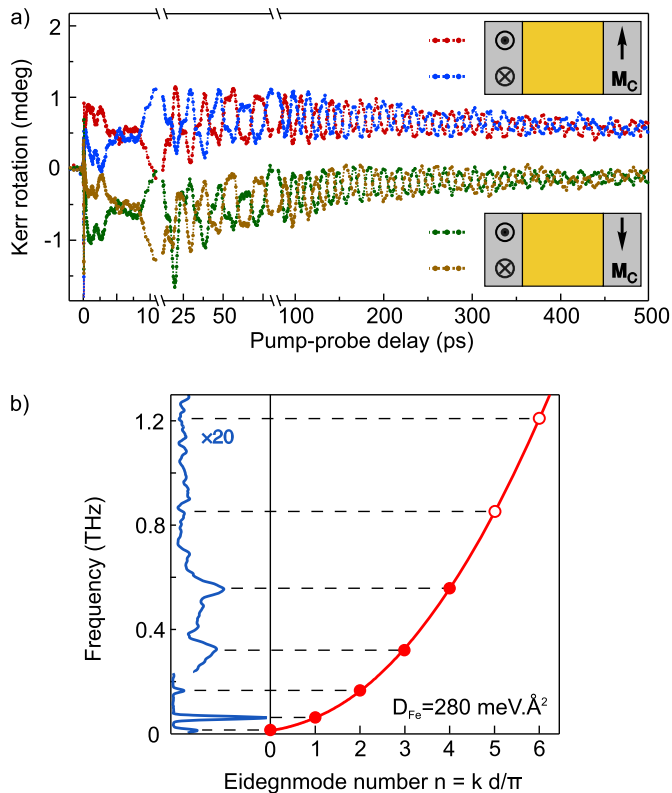


Fig. 13. (a) Time resolved MOKE measured in four different geometries depicted on the right handside. (b) Fourier spectrum of some similar measurements (left panel). The red line shows the calculated spin wave dispersion curve where D_{Fe} is the magnon stiffness (right panel). Adapted from [156].

in the Co layer is similar to the one lost in the [Co/Ni]. This raises question about the mechanism involved in the optical-STT and more specially on the generation of spin current by ultrashort laser pulse excitations.

The use of photoexcited hot-electrons was recently extended to reverse the magnetization in GdFeCo ferrimagnets [159,160]. Indeed, Wilson et al. reported that a single laser pulse could reverse the magnetization of GdFeCo buried below a thick Au layer [159]. They demonstrated that thermal currents were responsible for the magnetization reversal. Xu and collaborators studied the possibility to reverse the magnetization of GdFeCo using hot-electron excitation [160]. While the sample structures are quite similar in both studies, Xu et al., using Cu instead of Au, showed that the transport of hot-electrons generated in a Pt layer and propagating through the Cu layer was ballistic. Furthermore, magnetization reversal was observed in GdFeCo samples with a composition presenting a compensation temperature above or below room temperature, proving that one of the limiting factors for the observation of magnetization switching is the demagnetizing field that tends to break the uniformly magnetized sample into a multi-domain configuration. Moreover, comparing direct laser and hot-electrons excitations, it was demonstrated that both kind of excitations lead to the same magnetization reversal dynamics with

a complete reversal achieved in 40 ps. Finally, considering a bit of $20 \times 20 \times 10 \text{ nm}^3$, the switching energy was estimated to be about $\sim 4 \text{ fJ}$ [160], which is one order of magnitude lower than the one required in STT-MRAM [161].

A step forward in the implementation of fully integrated ultrafast spintronics was undertaken by Yang et al., who demonstrated ultrafast switching of GdFeCo by a single sub-10 ps electrical pulse generated by a photo-switch [162]. The energy density required to switch the magnetization is projected to be only $\sim 3.5 \text{ fJ}$ for a 20 nm^3 cell.

5 Conclusion and outlook

The field of laser induced ultrafast magnetization dynamics has been intensively studied during the last two decades. The accumulated knowledge has shown that several processes occur on the femtosecond time scale following laser excitation. It has swept away the idea of explaining the ultrafast demagnetization by a single microscopic mechanism. As a consequence, recent efforts were focused on the respective contributions of local and non-local mechanisms to dissipate the angular momentum during the ultrafast demagnetization. Among these mechanisms, this review aimed at exposing some of the major experimental and theoretical works that have specifically addressed the relevance of super-diffusive transport of spin polarized hot-electrons. This review also aimed at showing that optically generated hot-electrons and spin currents have opened new routes to manipulate the magnetization on the sub-picosecond time scale. These new exciting developments allow us to deepen our knowledge related to the ultrafast loss of magnetization, to modify the magnetization dynamics as well as manipulating magnetization through the ultrafast spin transfer torque.

Despite the recent advances presented in this review, different questions remain without answer. For instance, what are the spin-dependent scattering processes controlling superdiffusive spin transport? How do locally absorbed hot-electrons when injected into a ferromagnet interact with magnons or phonons? Does the spin diffusion length of photoexcited hot-electrons differ from the one measured at the Fermi energy? What is the role played by the interfaces? Can non-equilibrium spin current be filtered to improve the spin polarization? How would spin-polarized hot carriers interact with an insulating ferromagnet? And finally, would it be possible to reverse in a controlled way the magnetization of a ferromagnetic layer by injection of photoexcited spin-polarized hot-electrons?

We have restricted the topic of this review to the role of hot-electrons transport during laser induced ultrafast demagnetization and on how these optically generated hot-electrons and spin currents can be used to manipulate the magnetization on the sub-picosecond time-scale. However, no doubt that the capacities offered by optically excited hot-electrons in metals represent the next revolution in ultrafast spintronics and magnetization manipulation [163]. Among these perspectives, an extremely

exciting application of laser induced spin currents deals with THz emission [164]. Kampfarth et al. have excited ultrafast spin currents in a Fe layer with femtosecond laser pulses that they have injected into a non-magnetic capping layer [165]. Spin currents are then converted in intense and broadband THz electromagnetic pulses. By changing the metallic capping layer, they were able to modulate the emission spectrum of the induced THz radiation [165] and extend it up to 30 THz [166]. They concluded that the amplitudes of their THz emitters are only two order of magnitude smaller than standard THz sources. They foresee this gap could be overcome by optimizing the magnetic heterostructure. Huisman et al. have investigated the helicity-dependence of laser induced THz emission in similar magnetic heterostructures for a broader range of non-magnetic materials [167]. Furthermore, Spin injection in semi-conductor which possess longer spin diffusion length than metals is one of the major prospect to develop efficient spintronic devices. Recently, Battiato et al. have predicted that the excitation of mobile spin-polarized hot-electrons pulses in a Ni films by femtosecond laser pulses allows gigantic spin injection in a Si layer [168]. Even though some experimental issues exist, clear evidence of spin injection into Si has been reported [169]. However, an alternative system like Fe/GaAs might prove more promising since it is a well-known and established system which has been studied for almost 20 years [170].

This work was partly supported by the French PIA project Lorraine Universit dExcellence, reference ANR-15-IDEX-04-LUE, by the ANR-NSF Project, ANR-13-IS04-0008-01, COMAG and ANR-15-CE24-0009, UMAMI. This work was also partly funded by the ANRT, under the CIFRE convention 2016/1458 and by the Institut Carnot ICEEL for the project Optic-switch.

Author contribution statement

All the authors were involved in the preparation of the manuscript. All the authors have read and approved the final manuscript.

References

1. C.H. Back, D. Weller, J. Heidmann, D. Mauri, D. Guarisco, E.L. Garwin, H.C. Siegmann, *Phys. Rev. Lett.* **81**, 3251 (1998)
2. J. Katine, F. Albert, R. Buhrman, E. Myers, D. Ralph, *Phys. Rev. Lett.* **84**, 3149 (2000)
3. J. Grollier, D. Lacour, V. Cros, A. Hamzic, A. Vaures, A. Fert, D. Adam, G. Faini, *J. Appl. Phys.* **92**, 4825 (2002)
4. K. Uchida, S. Takahashi, K. Harii, J. Ieda, W. Koshibae, K. Ando, S. Maekawa, E. Saitoh, *Nature* **455**, 778 (2008)
5. G.E.W. Bauer, E. Saitoh, B.J. van Wees, *Nat. Mater.* **11**, 391 (2012)
6. Y. Shiota, T. Nozaki, F. Bonell, S. Murakami, T. Shinjo, Y. Suzuki, *Nat. Mater.* **11**, 39 (2012)
7. T. Nozaki, Y. Shiota, S. Miwa, S. Murakami, F. Bonell, S. Ishibashi, H. Kubota, K. Yakushiji, T. Saruya, A. Fukushima, S. Yuasa, T. Shinjo, Y. Suzuki, *Nat. Phys.* **8**, 492 (2012)
8. K. Roy, S. Bandyopadhyay, J. Atulasimha *Appl. Phys. Lett.* **99**, 063108 (2016)
9. C. Vicario, C. Ruchert, F. Ardana-Lamas, P.M. Derlet, B. Tudu, J. Luning, C.P. Hauri, *Nat. Photonics* **7**, 720 (2013)
10. T. Kubacka, J.A. Johnson, M.C. Hoffmann, C. Vicario, S. deJong, P. Beaud, S. Grubel, S.-W. Huang, L. Huber, L. Patthey, Y.-D. Chuang, J.J. Turner, G.L. Dakovski, W.-S. Lee, M.P. Minitti, W. Schlotter, R.G. Moore, C.P. Hauri, S.M. Koohpayeh, V. Scagnoli, G. Ingold, S.L. Johnson, U. Staub, *Science* **343**, 1333 (2014)
11. E. Beaupaire, J.-C. Merle, A. Daunois, J.-Y. Bigot, *Phys. Rev. Lett.* **76**, 4250 (1996)
12. C.D. Stanciu, F. Hansteen, A.V. Kimel, A. Kirilyuk, A. Tsukamoto, A. Itoh, Th. Rasing, *Phys. Rev. Lett.* **99**, 047601 (2007)
13. A. Kirilyuk, A.V. Kimel, Th. Rasing, *Rep. Prog. Phys.* **76**, 026501 (2013)
14. M.N. Baibich, J.M. Broto, A. Fert, F. Nguyen Van Dau, F. Petroff, P. Etienne, G. Creuzet, A. Friederich, J. Chazelas, *Phys. Rev. Lett.* **61**, 2472 (1988)
15. G. Binasch, P. Grünberg, F. Saurenbach, W. Zinn, *Phys. Rev. B* **39**, 4828 (1989)
16. J.S. Moodera, L.R. Kinder, T.M. Wong, R. Meservey, *Phys. Rev. Lett.* **74**, 3273 (1995)
17. D.J. Monsma, J.C. Loder, Th.J.A. Popma, B. Dieny, *Phys. Rev. Lett.* **74**, 5260 (1995)
18. K. Mizushima, T. Kinno, T. Yamauchi, K. Tanak, *IEEE Trans. Magn.* **33**, 3500 (1997)
19. W. Weber, S. Riesen, H.C. Siegmann, *Science* **291**, 1015 (2001)
20. R. Jansen, *J. Phys. D: Appl. Phys.* **36**, R289 (2003)
21. M. Bauer, A. Marienfeld, M. Aeschlimann, *Prog. Surf. Sci.* **90**, 319 (2015)
22. V.P. Zhukov, E.V. Chulkov, P.M. Echenique, *Phys. Rev. Lett.* **93**, 096401 (2004)
23. V. Zhukov, E. Chulkov, P. Echenique, *Phys. Rev. B* **72**, 155109 (2005)
24. V.P. Zhukov, E.V. Chulkov, P.M. Echenique, *Phys. Rev. B* **73**, 125105 (2006)
25. B. Koopmans, J.J.M. Ruigrok, F. Dalla Longa, W.J.M. deJonge, *Phys. Rev. Lett.* **95**, 267207 (2005)
26. B. Koopmans, G. Malinowski, F. Dalla Longa, D. Steiauf, M. Fähnle, T. Roth, M. Cinchetti, M. Aeschlimann, *Nat. Mater.* **9**, 259 (2010)
27. M. Krauß, T. Roth, S. Alebrand, D. Steil, M. Cinchetti, M. Aeschlimann, H.C. Schneider, *Phys. Rev. B* **80**, 180407 (2009)
28. M. Battiato, K. Carva, P.M. Oppeneer, *Phys. Rev. Lett.* **105**, 027203 (2010)
29. M. Battiato, K. Carva, P.M. Oppeneer, *Phys. Rev. B* **86**, 024404 (2012)
30. C. Rulliere, *Femtosecond laser pulses, principles and experiments*. Advanced texts in physics (Springer, New York, 2007)
31. G. Margaritondo, *Introduction to synchrotron radiation* (Oxford University Press, 1988)
32. K. Wille, *The physics of particle accelerators: an introduction* (Clarendon Press, 2000)

33. H.N. Chapman, A. Barty, M.J. Bogan, S. Boutet, M. Frank, S.P. Hau-Riege, S. Marchesini, B.W. Woods, S. Bajt, W.H. Benner, R.A. London, E. Plönjes, M. Kuhlmann, R. Treusch, S. Düsterer, T. Tschentscher, J.R. Schneider, E. Spiller, T. Möller, C. Bostedt, M. Hoener, D.A. Shapiro, K.O. Hodgson, D. vander Spoel, F. Burmeister, M. Bergh, C. Caleman, G. Huldt, M.M. Seibert, F.R.N.C. Maia, R.W. Lee, A. Szöke, N. Timneanu, J. Hajdu, *Nat. Phys.* **2**, 839 (2006)
34. A. Ravasio, D. Gauthier, F.R.N.C. Maia, M. Billon, J-P. Caumes, D. Garzella, M. Géléoc, O. Gobert, J-F. Hergott, A-M. Pena, H. Perez, B. Carré, E. Bourhis, J. Gierak, A. Madouri, D. Mailly, B. Schiedt, M. Fajardo, J. Gautier, P. Zeitoun, P.H. Bucksbaum, J. Hajdu, H. Merdji, *Phys. Rev. Lett.* **103**, 028104 (2009)
35. B. Koopmans, M. van Kampen, J.T. Kohlhepp, W.J.M. deJonge, *Phys. Rev. Lett.* **85**, 844 (2000)
36. T. Kampfrath, R. Ulbrich, F. Leuenberger, M. Müntenberg, B. Sass, W. Felsch, *Phys. Rev. B* **65**, 1 (2002)
37. L. Guidoni, E. Beaurepaire, J.-Y. Bigot, *Phys. Rev. Lett.* **89**, 017401 (2002)
38. E. Carpene, E. Mancini, C. Dallera, M. Brenna, E. Puppini, S. De Silvestri *Phys. Rev. B* **78**, 174422 (2008)
39. E. Carpene, H. Hedayat, F. Boschini, C. Dallera, *Phys. Rev. B* **91**, 174414 (2015)
40. I. Razdolski, A. Alekhin, U. Martens, D. Brstel, D. Diesing, M. Müntenberg, U. Bovensiepen, A. Melnikov, *J. Phys. Condens. Matter* **29**, 174002 (2017)
41. M. Van Kampen, C. Jozsa, J.T. Kohlhepp, P. LeClair, L. Lagae, W.J.M. De Jonge, B. Koopmans, *Phys. Rev. Lett.* **88**, 227201 (2002)
42. F. Dalla Longa, J.T. Kohlhepp, W.J.M. deJonge, B. Koopmans, *Phys. Rev. B* **75**, 224431 (2007)
43. G. Malinowski, F. Dalla Longa, J.H.H. Rietjens, P.V. Paluskar, R. Huijink, H.J.M. Swagten, B. Koopmans, *Nat. Phys.* **4**, 855 (2008)
44. J.-Y. Bigot, M. Vomer, E. Beaurepaire, *Nat. Phys.* **5**, 515 (2009)
45. J. Wieczorek, A. Eschenlohr, B. Weidtmann, M. Rösner, N. Berggard, A. Tarasevitch, T.O. Wehling, U. Bovensiepen, *Phys. Rev. B* **92**, 174410 (2015)
46. N. Berggard, M. Hehn, S. Mangin, G. Lengaigne, F. Montaigne, M.L.M. Laliou, B. Koopmans, G. Malinowski, *Phys. Rev. Lett.* **117**, 147203 (2016)
47. G. Salvatella, R. Gort, K. Bühlmann, S. Däster, A. Vaterlaus, Y. Acremann, *Struct. Dyn.* **3**, 7 (2016)
48. B. Koopmans, *Top. Appl. Phys.* **87**, 253 (2003)
49. M. Sultan, U. Atxitia, A. Melnikov, O. Chubykalo-Fesenko, U. Bovensiepen, *Phys. Rev. B* **85**, 184407 (2012)
50. M. Deb, P. Molho, B. Barbara, J.-Y. Bigot, *Phys. Rev. B* **94**, 054422 (2016)
51. J. Becker, A. Tsukamoto, A. Kirilyuk, J.C. Maan, Th. Rasing, P.C.M. Christianen, A.V. Kimel, *Phys. Rev. Lett.* **118**, 117203 (2017)
52. H. Ebert, *Rep. Prog. Phys.* **59**, 1665 (1996)
53. J.L. Erskine, E.A. Stern, *Phys. Rev. B* **8**, 1239 (1973)
54. I. Radu, G. Woltersdorf, M. Kiessling, A. Melnikov, U. Bovensiepen, J.-U. Thiele, C.H. Back, *Phys. Rev. Lett.* **102**, 117201 (2009)
55. A. Eschenlohr, M. Sultan, A. Melnikov, N. Berggard, J. Wieczorek, T. Kachel, C. Stamm, U. Bovensiepen, *Phys. Rev. B* **89**, 214423 (2014)
56. P. Hansen, C. Clausen, G. Much, M. Rosenkranz, K. Witter, *J. Appl. Phys.* **66**, 756 (1989)
57. P. Hansen, S. Klahn, C. Clausen, G. Much, K. Witter, *J. Appl. Phys.* **69**, 3194 (1991)
58. G. Cerullo, S. De Silvestri, *Rev. Sci. Instrum.* **74**, 1 (2003)
59. A.R. Khorsand, M. Savoini, A. Kirilyuk, A.V. Kimel, A. Tsukamoto, A. Itoh, Th. Rasing, *Phys. Rev. Lett.* **110**, 107205 (2013)
60. A. Hassdenteufel, C. Schubert, P. Reinhardt, P. Richter, M. Fronk, D.R.T. Zahn, R. Bratschitsch, G. Salvan, M. Albrecht, *J. Phys. D: Appl. Phys.* **48**, 245001 (2015)
61. A.J. Schellekens, N. deVries, J. Lucassen, B. Koopmans, *Phys. Rev. B* **90**, 104429 (2014)
62. A. Eschenlohr, J. Wieczorek, J. Chen, B. Weidtmann, M. Rösner, N. Berggard, A. Tarasevitch, T.O. Wehling, U. Bovensiepen, Analyzing ultrafast laser-induced demagnetization in Co/Cu(001) via the depth sensitivity of the time-resolved transversal magneto-optical Kerr effect, in *Proceedings of SPIE 9746, Ultrafast Phenomena Nanophotonics XX*, edited by M. Betz, A.Y. Elezabi (2016) p. 97461E
63. J. Hamrle, J. Ferré, M. Nývlt, Š. Višnovský, *Phys. Rev. B* **66**, 1 (2002)
64. J. Hohlfeld, E. Matthias, R. Knorren, K.H. Bennemann, *Phys. Rev. Lett* **78**, 4861 (1997)
65. A. Melnikov, O. Krupin, U. Bovensiepen, K. Starke, M. Wolf, E. Matthias, *Appl. Phys. B: Lasers Opt.* **74**, 723 (2002)
66. A. Kirilyuk, *J. Phys. D: Appl. Phys.* **35**, R189 (2002)
67. J. Güdde, U. Conrad, V. Jähnke, J. Hohlfeld, E. Matthias, *Phys. Rev. B* **59**, 6608 (1999)
68. H. Regensburger, R. Vollmer, J. Kirschner, *Phys. Rev. B* **61**, 716 (2000)
69. K.H. Bennemann, *J. Magn. Magn. Mater.* **200**, 679 (1999)
70. A. Melnikov, I. Razdolski, T.O. Wehling, E.Th. Papaioannou, V. Roddatis, P. Fumagalli, O. Aktsipetrov, A.I. Lichtenstein, U. Bovensiepen, *Phys. Rev. Lett.* **107**, 076601 (2011)
71. J. Chen, J. Wieczorek, A. Eschenlohr, S. Xiao, A. Tarasevitch, U. Bovensiepen, *Appl. Phys. Lett.* **110**, 092407 (2017)
72. U. Bovensiepen, *J. Phys. Condens. Matter* **19**, 083201 (2007)
73. M. Sultan, A. Melnikov, U. Bovensiepen, *Phys. Status Solidi B* **248**, 2323 (2011)
74. M. Protopapas, C.H. Keitel, P.L. Knight, *Rep. Prog. Phys.* **60**, 389 (1997)
75. T. Pfeifer, C. Spielmann, G. Gerber, *Rep. Prog. Phys.* **69**, 443 (2006)
76. T. Fan, P. Grychtol, R. Knut, C. Hernández-García, D.D. Hickstein, D. Zusin, C. Gentry, F.J. Dollar, C.A. Mancuso, C.W. Hogle, O. Kfir, D. Legut, K. Carva, J.L. Ellis, K.M. Dorney, C. Chen, O.G. Shpyrko, E.E. Fullerton, O. Cohen, P.M. Oppeneer, D.B. Milošević, A. Becker, A.A. Jaroń-Becker, T. Popmintchev, M.M. Murnane, H.C. Kapteyn, *Proc. Natl. Acad. Sci. USA* **112**, 14206 (2015)
77. C. La-O-Vorakiat, M. Siemens, M.M. Murnane, H.C. Kapteyn, S. Mathias, M. Aeschlimann, P. Grychtol, R. Adam, C.M. Schneider, J.M. Shaw, H. Nembach, T.J. Silva, *Phys. Rev. Lett.* **103**, 257402 (2009)
78. S. Mathias, C. La-O-Vorakiat, P. Grychtol, P. Granitzka, E. Turgut, J.M. Shaw, R. Adam, H.T. Nembach,

- M.E. Siemens, S. Eich, C.M. Schneider, T.J. Silva, M. Aeschlimann, M.M. Murnane, H.C. Kapteyn, *Proc. Natl. Acad. Sci. USA* **109**, 4792 (2012)
79. A. Fleischer, O. Kfir, T. Diskin, P. Sidorenko, O. Cohen, *Nat. Photonics* **8**, 543 (2014)
80. A. Ferré, C. Handschin, M. Dumergue, F. Burgy, A. Comby, D. Descamps, B. Fabre, G.A. Garcia, R. Géneaux, L. Merceron, E. Mével, L. Nahon, S. Petit, B. Pons, D. Staedter, S. Weber, T. Ruchon, V. Blanchet, Y. Mairesse, *Nat. Photonics* **9**, 93 (2014)
81. G. Lambert, B. Vodungbo, J. Gautier, B. Mahieu, V. Malka, S. Sebban, P. Zeitoun, J. Luning, J. Perron, A. Andreev, S. Stremoukhov, F. Ardana-Lamas, A. Dax, C.P. Hauri, A. Sardinha, M. Fajardo, *Nat. Commun.* **6**, 6167 (2015)
82. S. Stremoukhov, A. Andreev, B. Vodungbo, P. Salières, B. Mahieu, G. Lambert, *Phys. Rev. A* **94**, 013855 (2016)
83. F. Willems, C.T.L. Smeenk, N. Zhavoronkov, O. Kornilov, I. Radu, M. Schmidbauer, M. Hanke, C. Von Korff Schmising, M.J.J. Vrakking, S. Eisebitt, *Phys. Rev. B* **92**, 220405 (2015)
84. R. Carley, K. Döbrich, B. Frietsch, C. Gahl, M. Teichmann, O. Schwarzkopf, P. Wernet, M. Weinelt, *Phys. Rev. Lett.* **109**, 057401 (2012)
85. B. Frietsch, R. Carley, K. Döbrich, C. Gahl, M. Teichmann, O. Schwarzkopf, P. Wernet, M. Weinelt, *Rev. Sci. Instrum.* **84**, 075106 (2013)
86. B. Frietsch, J. Bowlan, R. Carley, M. Teichmann, S. Wienholdt, D. Hinzke, U. Nowak, K. Carva, P.M. Oppeneer, M. Weinelt, *Nat. Commun.* **6**, 8262 (2015)
87. D. Weller, J. Stöhr, R. Nakajima, A. Carl, M.G. Samant, C. Chappert, R. Mégy, P. Beauvillain, P. Veillet, G.A. Held, *Phys. Rev. Lett.* **75**, 3752 (1995)
88. J. Stohr, *J. Magn. Magn. Mater.* **200**, 470 (1999)
89. A. Agui, M. Mizumaki, T. Asahi, K. Matsumoto, T. Morikawa, J. Sayama, T. Osaka, *J. Phys. Chem. Solids* **68**, 2148 (2007)
90. I. Radu, C. Stamm, A. Eschenlohr, F. Radu, R. Abrudan, K. Vahaplar, T. Kachel, N. Pontius, R. Mitzner, K. Holldack, A. Föhlisch, T.A. Ostler, J.H. Mentink, R.F.L. Evans, R.W. Chantrell, A. Tsukamoto, A. Itoh, A. Kirilyuk, A.V. Kimel, *Th. Rasing, SPIN* **5**, 1550004 (2015)
91. K. Chen, D. Lott, F. Radu, F. Choueikani, E. Otero, P. Ohresser, *Phys. Rev. B* **91**, 024409 (2015)
92. P. Carra, B.T. Thole, M. Altarelli, X. Wang, *Phys. Rev. Lett.* **69**, 2013 1992
93. B.T. Thole, P. Carra, F. Sette, G. Van Der Laan, *Phys. Rev. Lett.* **68**, 1943 1992
94. C. Chen, Y. Idzerda, H.-J. Lin, N. Smith, G. Meigs, E. Chaban, G. Ho, E. Pellegrin, F. Sette, *Phys. Rev. Lett.* **75**, 152 (1995)
95. S. Mangin, C. Bellouard, S. Andrieu, F. Montaigne, P. Ohresser, N. Brookes, B. Barbara, *Phys. Rev. B* **70**, 014401 (2004)
96. A. Zholents, M. Zolotarev, *Phys. Rev. Lett.* **76**, 912 (1996)
97. S. Khan, K. Holldack, T. Kachel, R. Mitzner, T. Quast, *Phys. Rev. Lett.* **97**, 074801 (2006)
98. K. Holldack, J. Bahrtdt, A. Balzer, U. Bovensiepen, M. Brzhezinskaya, A. Erko, A. Eschenlohr, R. Follath, A. Firsov, W. Frentrup, L. Le Guyader, T. Kachel, P. Kuske, R. Mitzner, R. Mueller, N. Pontius, T. Quast, I. Radu, J.S. Schmidt, C. Schuessler-Langeheine, M. Sperling, C. Stamm, C. Trabant, A. Foehlich, *J. Synchrotron Radiat.* **21**, 1090 (2014)
99. T. Kachel, F. Eggenstein, R. Follath, *J. Synchrotron Radiat.* **22**, 1301 (2015)
100. C. Stamm, T. Kachel, N. Pontius, R. Mitzner, T. Quast, K. Holldack, S. Khan, C. Lupulescu, E.F. Aziz, M. Wietstruk, H.A. Dürr, W. Eberhardt, *Nat. Mater.* **6**, 740 (2007)
101. K. Carva, D. Legut, P.M. Oppeneer, *Europhys. Lett.* **86**, 57002 (2009)
102. C. Boeglin, E. Beaurepaire, V. Halte, V. Lopez-Flores, C. Stamm, N. Pontius, H.A. Dürr, J.-Y. Bigot, *Nature* **465**, 458 (2010)
103. N. Bergeard, V. López-Flores, V. Halté, M. Hehn, C. Stamm, N. Pontius, E. Beaurepaire, C. Boeglin, *Nat. Commun.* **5**, 3466 (2014)
104. M. Wietstruk, A. Melnikov, C. Stamm, T. Kachel, N. Pontius, M. Sultan, C. Gahl, M. Weinelt, H.A. Dürr, U. Bovensiepen, *Phys. Rev. Lett.* **106**, 127401 (2011)
105. I. Radu, K. Vahaplar, C. Stamm, T. Kachel, N. Pontius, H.A. Dürr, T.A. Ostler, J. Barker, R.F.L. Evans, R.W. Chantrell, A. Tsukamoto, A. Itoh, A. Kirilyuk, Th. Rasing, A.V. Kimel, *Nature* **472**, 205 (2011)
106. D.J. Higley, K. Hirsch, G.L. Dakovski, E. Jal, E. Yuan, T. Liu, A.A. Lutman, J.P. Macarthur, E. Arenholz, Z. Chen, G. Coslovich, P. Denes, P.W. Granitzka, P. Hart, M.C. Hoffmann, J. Joseph, L. Le Guyader, A. Mitra, S. Moeller, H. Ohldag, M. Seaberg, P. Shafer, J. Stöhr, A. Tsukamoto, H.-D. Nuhn, A.H. Reid, H.A. Dürr, W.F. Schlotter, *Rev. Sci. Instrum.* **87**, 033110 (2016)
107. K. Holldack, N. Pontius, E. Schierle, T. Kachel, V. Soltwisch, R. Mitzner, T. Quast, G. Springholz, E. Weschke, *Appl. Phys. Lett.* **97**, 062502 (2010)
108. E. Jal, V. López-Flores, N. Pontius, C. Schuessler-Langeheine, T. Ferté, N. Bergeard, C. Boeglin, B. Vodungbo, J. Lüning, N. Jaouen, *Phys. Rev. B* **95**, 184422 (2017)
109. A. Von Reppert, J.Pudell, A. Koc, M. Reinhardt, W. Leitenberger, K. Dumesnil, F. Zamponi, M. Bargheer, *Struct. Dyn.* **3**, 054302 (2016)
110. L. Rettig, C. Dornes, N. Thielemann-Kühn, N. Pontius, H. Zabel, D.L. Schlagel, T.A. Lograsso, M. Chollet, A. Robert, M. Sikorski, S. Song, J.M. Glowina, C. Scuessler-Langeheine, S.L. Johnson, U. Staub, *Phys. Rev. Lett.* **116**, 257202 (2016)
111. B. Vodungbo, J. Gautier, G. Lambert, A. Barszczak Sardinha, M. Lozano, S. Sebban, M. Ducouso, W. Boutu, K. Li, B. Tudu, M. Tortarolo, R. Hawaldar, R. Delaunay, V. Lopez-Flores, J. Arabski, C. Boeglin, H. Merdji, P. Zeitoun, J. Luning, *Nat. Commun.* **3**, 999 (2012)
112. B. Pfau, S. Schaffert, L. Müller, *Nat. Commun.* **3**, 1100 (2012)
113. L.H. Yu, *Phys. Rev. A* **44**, 5178 (1991)
114. P. Cinquegrana, S. Cleva, A. Demidovich, G. Gaio, R. Ivanov, G. Kurdi, I. Nikolov, P. Sigalotti, M.B. Danailov, *Phys. Rev. Special Topics Accel. Beams* **17**, 040702 (2014)
115. M.B. Danailov, F. Bencivenga, F. Capotondi, F. Casolari, P. Cinquegrana, A. Demidovich, E. Giangrisostomi, M.P. Kiskinova, G. Kurdi, M. Manfreda, C. Masciovecchio, R. Mincigrucci, I.P. Nikolov, E. Pedersoli, E. Principi, P. Sigalotti, *Opt. Express* **22**, 12869 (2014)
116. T. Maltezopoulos, S. Cunovic, M. Wieland, M. Beye, A. Azima, H. Redlin, M. Krikunova, R. Kalms, U. Fruehling,

- F. Budzyn, W. Wurth, A. Foehlich, M. Drescher, *New J. Phys.* **10**, 033026 (2008)
117. S. Schorb, T. Gorkhover, J.P. Cryan, J.M. Glownia, M.R. Bionta, R.N. Coffee, B. Erk, R. Boll, C. Schmidt, D. Rolles, A. Rudenko, A. Rouzee, M. Swiggers, S. Carron, J.C. Castagna, J.D. Bozek, M. Messerschmidt, W.F. Schlotter, C. Bostedt, *Appl. Phys. Lett.* **100**, 121107 (2012)
118. M. Harmand, R. Coffee, M.R. Bionta, M. Chollet, D. French, D. Zhu, D.M. Fritz, H.T. Lemke, N. Medvedev, B. Ziaja, S. Toleikis, M. Cammarata, *Nat. Photonics* **7**, 215 (2013)
119. H.-S. Kang, C.-K. Min, H. Heo, C. Kim, H. Yang, G. Kim, I. Nam, S.Y. Baek, H.-J. Choi, G. Mun, B.R. Park, Y.J. Suh, D.C. Shin, J. Hu, J. Hong, S. Jung, S.-H. Kim, K.H. Kim, D. Na, S.S. Park, Y.J. Park, J.-H. Han, Y.G. Jung, S.H. Jeong, H.G. Lee, S. Lee, S. Lee, W.-W. Lee, B. Oh, H.S. Suh, Y.W. Parc, S.-J. Park, M.H. Kim, N.-S. Jung, Y.-C. Kim, B.H. Lee, M.-S. Lee, C.-W. Sung, I.-S. Mok, J.-M. Yang, C.-S. Lee, H. Shin, J.H. Kim, Y. Kim, J.H. Lee, J. Park, S.-Y. Kim, J. Park, I. Eom, S. Rah, S. Kim, K.H. Nam, J. Park, J. Park, S. Kim, S. Kwon, S.H. Park, K.S. Kim, H. Hyun, S.N. Kim, S. Kim, S.-M. Hwang, M.J. Kim, C.-Y. Lim, C.-J. Yu, B.-S. Kim, T.-H. Kang, K.-W. Kim, S.-H. Kim, H.-S. Lee, H.-S. Lee, K.-H. Park, T.-Y. Koo, D.-E. Kim, I.S. Ko, *Nat. Photonics* **11**, 708 (2017)
120. N. Bergéard, S. Schaffert, V. López-Flores, N. Jaouen, J. Geilhufe, C.M. Günther, M. Schneider, C. Graves, T. Wang, B. Wu, A. Scherz, C. Baumier, R. Delaunay, F. Fortuna, M. Tortarolo, B. Tudu, O. Krupin, M.P. Minitti, J. Robinson, W.F. Schlotter, J.J. Turner, J. Lüning, S. Eisebitt, C. Boeglin, *Phys. Rev. B* **91**, 054416 (2015)
121. B. Vodungbo, B. Tudu, J. Perron, R. Delaunay, L. Müller, M.H. Berntsen, G. Grübel, G. Malinowski, C. Weier, J. Gautier, G. Lambert, P. Zeitoun, C. Gutt, E. Jal, A.H. Reid, P.W. Granitzka, N. Jaouen, G.L. Dakovski, S. Moeller, M.P. Minitti, A. Mitra, S. Carron, B. Pfau, C. von Korff Schmising, M. Schneider, S. Eisebitt, J. Lüning, *Sci. Rep.* **6**, 18970 (2016)
122. C.E. Graves, A.H. Reid, T. Wang, B. Wu, S. deJong, K. Vahaplar, I. Radu, D.P. Bernstein, M. Messerschmidt, L. Müller, R. Coffee, M. Bionta, S.W. Epp, R. Hartmann, N. Kimmel, G. Hauser, A. Hartmann, P. Holl, H. Gorke, J.H. Mentink, A. Tsukamoto, A. Fognini, J.J. Turner, W.F. Schlotter, D. Rolles, H. Soltau, L. Strüder, Y. Acremann, A.V. Kimel, A. Kirilyuk, Th. Rasing, J. Stöhr, A.O. Scherz, H.A. Dürr, *Nat. Mater.* **12**, 293 (2013)
123. W. Eberhardt, S. Eisebitt, J. Lüning, W.F. Schlotter, O. Hellwig, J. Stöhr, *Nature* **432**, 885 (2004)
124. D. Gauthier, M. Guizar-Sicairos, X. Ge, W. Boutu, B. Carré, J.R. Fienup, H. Merdji, *Phys. Rev. Lett.* **105**, 093901 (2010)
125. T. Wang, D. Zhu, B. Wu, C. Graves, S. Schaffert, T. Rander, L. Müller, B. Vodungbo, C. Baumier, D.P. Bernstein, B. Bräuer, V. Cros, S. deJong, R. Delaunay, A. Fognini, R. Kukreja, S. Lee, V. López-Flores, J. Mohanty, B. Pfau, H. Popescu, M. Sacchi, A.B. Sardinha, F. Sirotti, P. Zeitoun, M. Messerschmidt, J.J. Turner, W.F. Schlotter, O. Hellwig, R. Mattana, N. Jaouen, F. Fortuna, Y. Acremann, C. Gutt, H.A. Dürr, E. Beaurepaire, C. Boeglin, S. Eisebitt, G. Grübel, J. Lüning, J. Stöhr, A.O. Scherz, *Phys. Rev. Lett.* **108**, 267403 (2012)
126. C. von Korff Schmising, B. Pfau, M. Schneider, C.M. Günther, M. Giovannella, J. Perron, B. Vodungbo, L. Müller, F. Capotondi, E. Pedersoli, N. Mahne, J. Lüning, S. Eisebitt, *Phys. Rev. Lett.* **112**, 217203 (2014)
127. D.M. Nenno, S. Kaltenborn, H.C. Schneider, *Phys. Rev. B* **94**, 115102 (2016)
128. H. Vonesch, J.-Y. Bigot, *Phys. Rev. B* **85**, 180407 (2012)
129. M. Cinchetti, M. Sánchez Albaneda, D. Hoffmann, T. Roth, J.-P. Wüstenberg, M. Krauß, O. Andreyev, H.C. Schneider, M. Bauer, M. Aeschlimann, *Phys. Rev. Lett.* **97**, 177201 (2006)
130. K. Carva, M. Battiato, P.M. Oppeneer, *Phys. Rev. Lett.* **107**, 207201 (2011)
131. A.B. Schmidt, M. Pickel, M. Donath, P. Buczek, A. Ernst, V.P. Zhukov, P.M. Echenique, L.M. Sandratskii, E.V. Chulkov, M. Weinelt, *Phys. Rev. Lett.* **105**, 197401 (2010)
132. S. Essert, H.C. Schneider, *Phys. Rev. B* **84**, 224405 (2011)
133. K. Carva, M. Battiato, D. Legut, P.M. Oppeneer, *Phys. Rev. B* **87**, 184425 (2013)
134. B.Y. Mueller, A. Baral, S. Vollmar, M. Cinchetti, M. Aeschlimann, H.C. Schneider, B. Rethfeld, *Phys. Rev. Lett.* **111**, 167204 (2013)
135. U. Atxitia, O. Chubykalo-Fesenko, J. Walowski, A. Mann, M. Münzenberg, *Phys. Rev. B* **81**, 174401 (2010)
136. N. Kazantseva, U. Nowak, R.W. Chantrell, J. Hohlfeld, A. Rebei, *Europhys. Lett.* **81**, 27004 (2008)
137. S.D. Brorson, J.G. Fujimoto, E.P. Ippen, *Phys. Rev. Lett.* **59**, 1962 (1987)
138. T. Juhasz, H.E. Elsayed-Ali, G.O. Smith, C. Suárez, W.E. Bron, *Phys. Rev. B* **48**, 15488 (1993)
139. J. Hohlfeld, S.S. Wellershoff, J. Güdde, U. Conrad, V. Jähnke, E. Matthias, *Chem. Phys.* **251**, 237 (2000)
140. A.J. Schellekens, W. Verhoeven, T.N. Vader, B. Koopmans, *Appl. Phys. Lett.* **102**, 252408 (2013)
141. V. Shokeen, M. Sanchez Piaia, J.-Y. Bigot, T. Müller, P. Elliott, J.K. Dewhurst, S. Sharma, E.K.U. Gross, *Phys. Rev. Lett.* **119**, 107203 (2017)
142. M. Hofherr, P. Maldonado, O. Schmitt, M. Berritta, U. Bierbrauer, S. Sadashivaiah, A.J. Schellekens, B. Koopmans, D. Steil, M. Cinchetti, B. Stadtmüller, P.M. Oppeneer, S. Mathias, M. Aeschlimann, *Phys. Rev. B* **96**, 100403 (2017)
143. W. He, T. Zhu, X.-Q. Zhang, H.-T. Yang, Z.-H. Cheng, *Sci. Rep.* **3**, 2883 (2013)
144. E. Turgut, C. La-o vorakiat, J.M. Shaw, P. Grychtol, H.T. Nembach, D. Rudolf, R. Adam, M. Aeschlimann, C.M. Schneider, T.J. Silva, M.M. Murnane, H.C. Kapteyn, S. Mathias, *Phys. Rev. Lett.* **110**, 197201 (2013)
145. D. Rudolf, C. La-O-Vorakiat, M. Battiato, R. Adam, J.M. Shaw, E. Turgut, P. Maldonado, S. Mathias, P. Grychtol, H.T. Nembach, T.J. Silva, M. Aeschlimann, H.C. Kapteyn, M.M. Murnane, C.M. Schneider, P.M. Oppeneer, *Nat. Commun.* **3**, 1037 (2012)
146. K.C. Kuiper, T. Roth, A.J. Schellekens, O. Schmitt, B. Koopmans, M. Cinchetti, M. Aeschlimann, *Appl. Phys. Lett.* **105**, 202402 (2014)
147. A. Eschenlohr, M. Battiato, P. Maldonado, N. Pontius, T. Kachel, K. Holldack, R. Mitzner, A. Föhlisch, P.M. Oppeneer, C. Stamm, *Nat. Mater.* **12**, 332 (2013)

148. M. Battiato, G. Barbalinardo, K. Carva, P.M. Oppeneer, *Phys. Rev. B* **85**, 045117 (2012)
149. A.R. Khorsand, M. Savoini, A. Kirilyuk, Th. Rasing, *Nat. Mater.* **13**, 101 (2014)
150. L. Berger, *Phys. Rev. B* **54**, 9353 (1996)
151. J.C. Slonczewski, *J. Magn. Magn. Mater.* **159**, L1 (1996)
152. G.-M. Choi, B.-C. Min, K.-J. Lee, D.G. Cahill, *Nat. Commun.* **5**, 4334 (2014)
153. G.-M. Choi, C.-H. Moon, B.-C. Min, K.-J. Lee, D.G. Cahill, *Nat. Phys.* **11**, 576 (2015)
154. A.J. Schellekens, K.C. Kuiper, R.R.J.C. deWit, B. Koopmans, *Nat. Commun.* **5**, 4333 (2014)
155. G.-M. Choi, R.B. Wilson, D.G. Cahill, *Phys. Rev. B* **89**, 064307 (2014)
156. I. Razdolski, A. Alekhin, N. Ilin, J.P. Meyburg, V. Roddatis, D. Diesing, U. Bovensiepen, A. Melnikov, *Nat. Commun.* **8**, 15007 (2017)
157. A. Alekhin, I. Razdolski, N. Ilin, J.P. Meyburg, D. Diesing, V. Roddatis, I. Rungger, M. Stamenova, S. Sanvito, U. Bovensiepen, A. Melnikov, *Phys. Rev. Lett.* **119**, 017202 (2017)
158. M.L.M. Laliou, P.L.J. Helgers, B. Koopmans, *Phys. Rev. B* **96**, 014417 (2017)
159. R.B. Wilson, J. Gorchon, Y. Yang, C.-H. Lambert, S. Salahuddin, J. Bokor, *Phys. Rev. B* **95**, 180409 (2017)
160. Y. Xu, M. Deb, G. Malinowski, M. Hehn, W. Zhao, S. Mangin, *Adv. Mater.* **29**, 1703474 (2017)
161. J.P. Liu, E. Fullerton, O. Gutfleisch, D.J. Sellmyer, *Nanoscale magnetic materials applications* (Springer US, 2009)
162. Y. Yang, R.B. Wilson, J. Gorchon, C.-H. Lambert, S. Salahuddin, J. Bokor, *Sci. Adv.* **3**, e1603117 (2017)
163. K. Carva, *Nat. Phys.* **10**, 552 (2014)
164. J. Walowski, M. Münzenberg, *J. Appl. Phys.* **120**, 140901 (2016)
165. T. Kampfrath, M. Battiato, P. Maldonado, G. Eilers, J. Nötzold, S. Mährlein, V. Zbarsky, F. Freimuth, Y. Mokrousov, S. Blügel, M. Wolf, I. Radu, P.M. Oppeneer, M. Münzenberg, *Nat. Nanotechnol.* **8**, 256 (2013)
166. T. Seifert, S. Jaiswal, U. Martens, J. Hannegan, L. Braun, P. Maldonado, F. Freimuth, A. Kronenberg, J. Henzli, I. Radu, E. Beaupaire, Y. Mokrousov, P.M. Oppeneer, M. Jourdan, G. Jakob, D. Turchinovich, L.M. Hayden, M. Wolf, M. Münzenberg, M. Kläui, T. Kampfrath, *Nat. Photonics* **10**, 483 (2016)
167. T.J. Huisman, R.V. Mikhaylovskiy, J.D. Costa, F. Freimuth, E. Paz, J. Ventura, P.P. Freitas, S. Blügel, Y. Mokrousov, Th. Rasing, A.V. Kimel, *Nat. Nanotechnol.* **11**, 455 (2016)
168. M. Battiato, K. Held, *Phys. Rev. Lett.* **116**, 196601 (2016)
169. I. Appelbaum, B. Huang, D.J. Monsma, *Nature* **447**, 295 (2007)
170. H.J. Zhu, M. Ramsteiner, H. Kostial, M. Wassermeier, H.P. Schönherr, K.H. Ploog, *Phys. Rev. Lett.* **87**, 016601 (2001)